applied sciences

MDPI

Systematic Review

Advances and Applications of Three-Dimensional-Printed Patient-Specific Chest Phantoms in Radiology A Systematic Review

Jenna Silberstein [1] and Zhonghua Sun [1,2]

[1] Discipline of Medical Radiation Science, Curtin Medical School, Curtin University, Perth 6845, Australia; jenna.beinart@student.curtin.edu.au (J.S.)
[2] Curtin Health Innovation Research Institute (CHIRI), Curtin University, Perth 6845, Australia
* Correspondence: z.sun@curtin.edu.au; Tel.: +61-8-9266-7509

Abstract: Lung cancer screening would benefit from low-dose CT protocols optimized by means of a highly accurate three-dimensional radiation-equivalent thoracic phantom. However, it is unclear whether three-dimensional (3D) printed chest phantoms have been used for this purpose, nor their current scope of application. This systematic review aims to explore the range of applications of 3D printed thoracic phantoms, along with the techniques, materials, and anatomical structures they replicate. Relevant articles were identified using a systematic search strategy across PubMed and Scopus databases, based on pre-determined selection criteria. In total, 20 articles were eligible and critically analysed, all consisting of phantom experiments. Findings reveal that a diverse range of thoracic organs have been 3D printed, predominantly via fused-deposition modelling incorporating polylactic-acid, however, often representing discreet or limited structures. A comprehensive radiation-equivalent chest phantom that mimics the full gamut of thoracic structures, is warranted. Most studies are still in their preliminary testing stages, primarily assessing the feasibility of creating morphologically accurate thoracic structures with radiation equivalence. Few studies have progressed to explore their applications. Notably, most investigations into applications have concentrated on dose reduction and CT protocol optimisation for cardiac purposes, rather than pulmonary applications, despite the inclusion of lung cancer nodules in some phantoms.

Keywords: three-dimensional printing, additive manufacturing, fused-deposition modelling, thorax, patient-derived phantom, tissue-equivalence, radiation attenuation equivalence, lung cancer, lung nodule.

Citation: To be added by editorial staff during production.

Academic Editor: Firstname Lastname

Received: date
Revised: date
Accepted: date
Published: date

1. Introduction

Three-dimensional (3D) printing is an emerging technology that has found application in a diverse array of medical arenas [1]. Also coined “additive manufacturing”, 3D printing involves the successive layering or curing of printing materials according to a digital blueprint, to rapidly form an intricate three-dimensional prototype [2]. Its ability to accurately replicate anatomical detail has allowed it to serve as guidance for surgical planning and complement medical education and comprehension, benefiting doctors, healthcare professionals, students, and patients alike [1,3]. Additionally, 3D printing is invaluably used for fabricating and sizing of prosthetics in the maxillofacial and orthopaedic fields [4].

Customised, patient-specific models are increasingly utilised through harnessing 3D printing technology in radiology [1]. Medical imaging datasets including computed tomography (CT), magnetic resonance imaging (MRI) and ultrasound (US) images are converted to 3D standard tessellation language (STL) files from which the prototype is derived [5]. Three-dimensional printed anthropomorphic phantoms have garnered attention as a cost-effective, more realistic alternative to commercial phantoms used in the medical imaging field [6].

Commercial phantoms such as the anthropomorphic Alderson Rando phantom, and ATOM [7], have been criticised for their generalised non-personalised nature, limited access, and high cost associated with large machining facilities required to create them [6]. Other commercial phantoms include simple shaped slabs made of acrylic or ceramic materials, offering limited accuracy, and representing an expensive solution [8]. Conversely, 3D printed phantoms, being patient-derived and precisely deposited, can accurately mimic the true morphology and radiation attenuating properties of humans. Dedicated selection of materials that have similar compositions and electron densitieseffective atomic numbers and mass densities to human tissues can enhance radiation attenuation equivalence improving the accuracy of these phantoms [9]. Thus, researchers, radiologists, radiographers, and patients can better trust and rely on the accuracy of these phantoms in dosimetry, quality assurance studies and evaluating scanning protocols. Moreover, the widespread availability of 3D printers and printing materials [109] have facilitated greater access and faster creation of phantom models at lower costs to effectively serve the medical imaging community.

Formatted: Font color: Auto

Three-dimensional printed phantoms, including of the head, thorax, breast, lung, heart, thyroid, vessels, pelvis, liver, spine and abdomen, have been created and investigated as viable options created for dosimetry and quality assurance purposeses in medical imaging and radiation therapy –applicationstreatment and planning [6, 1110-17]. Others have been manufactured for optimising medical imaging protocols such as via a coronary artery model for optimising low dose CT coronary angiography protocols [181], a breast phantom for evaluating MRI protocols and quality assurance [192], and a patient-specific three-dimensional printed femur phantom for evaluation of noise reduction algorithms to enable low dose CT protocols for fracture detection –[2013], as well as a phantom for optimising low dose CT examinations to detect pelvic tumours [21].

Commercial phantoms are primarily utilized to optimize low dose CT (LDCT) protocols for lung cancer screening [2214,2315]. However, these phantoms are not truly anthropomorphic with regard to the condition/lesion to be identified, as is the case with 3D printed phantoms, which are directly derived from patient data [16] reliability is the main concern in these studies due to the lack of translatability of these findings to real patients, as would be instilled by 3D patient-specific phantoms. Furthermore, despite the multinational guidelines and evidence into the benefit of LDCT for early detection of lung nodules and thus, improved survival rates, many countries are hesitant to introduce and engage with national lung cancer screening programs due to the increased risk associated with higher levels of ionising radiation compared to conventional chest X-rays [2316]. With rapid advancements in CT and evolution of advanced technologies, evaluating lower dose protocols is timely [24, 25]. Using 3D printed chest phantoms as an alternative to commercial phantoms, may offer superior evaluation of low dose CT protocols for lung cancer screening. However, the development of 3D printed lung phantoms specifically for this purpose appears to be an area of inquiry research that is currently lackingunexplored.

Thus, the aim of this systematic review is to address the question: Are 3D printed chest phantoms currently addressed in the literature? for optimising CT protocols for lung cancer screening? What are the current applications of 3D printed chest phantoms and their methods of manufacture?

2. Materials and Methodologys

2.1. Search Strategy

A comprehensive literature search was conducted following the Preferred Reporting for Systematic Reviews and Meta-Analysis Guidelines [2717]. Two main databases, PubMed, and Scopus were searched using the search strategy presented in table 1.

Formatted: Font color: Auto

Formatted: Indent: Left: 0 cm, First line: 0 cm

Table 1. Search strategy used to identify eligible studies for inclusion in the review.

3D printing keyword (Title search)		**Lung keyword (Title & Abstract search)**		**Phantom keyword (Full text search)**
3D printing OR 3D printed OR 3D-printed OR 3D-printing OR 3-D-printed OR 3-dimensional Printing OR Three-dimensional printing OR three-dimensional printing OR three-dimensional (3D) printing OR three-dimensional (3-D) printer OR 3D printable OR 3D printer OR Additively Manufactured OR Additively manufacturing OR fused deposition modelling OR FDM OR Selective laser sintering OR SLS OR MultiJet printing OR PolyJet Printing OR Resin-based Vat photopolymerization OR vat polymerisation OR Vat polymerization OR VPP.	AND	lung OR pulmonary OR chest OR thorax OR bronchial OR respiratory OR alveoli OR alveolar OR lungs OR pleura OR thoracic	AND	phantom OR simulation OR Model OR Patient-replica OR construction OR design OR fabrication OR Patient-specific OR replica OR replication OR reproduction OR mould

2.2. *Inclusion and Exclusion Criteria*

Reports were included if they were original, full-text peer-reviewed articles, written in English and published in the last six years exploring the use of 3D-printed anthropomorphic phantoms of chest anatomy in CT medical imaging. The six-year time constraint was applied to enable recency of the acquired articles, especially pertinent considering the rapid progress of 3D printing technology within the last decade [2818]. Articles were further excluded if they were exclusively examining phantom models for radiotherapy application with no mention of medical imaging or radiology, if they were based on modalities other than CT, or represented phantoms that were not true to size replicas of human anatomy. Furthermore, phantoms that were for surgical guidance were excluded as they most likely do not represent true tissue radiodensities for medical imaging purposes. Grey literature such as conference papers, letter to editors, books, practice guidelines as well as pre-prints and case reports were additionally excluded.

2.3. Article Selection and Quality Assessment

After both databases were searched, duplicates were removed. The remaining articles were screened via title and excluded if the title did not explicitly indicate the study was examining phantom or models that represent chest anatomy. Abstracts were subsequently screened, and articles removed if they did not indicate CT as the modality of application. Full-text articles were then screened, and articles removed if they did not mention medical imaging or radiology. An additional four articles were identified as eligible from the reference lists of the included studies. This led to a total of 20 articles that were included in the review (Figure 1). Quality of each article was assessed using the Crowe Critical Appraisal Tool (CCAT) v1.4 which has been validated as a comprehensive and reliable tool for evaluating a diverse range of research designs [2919].

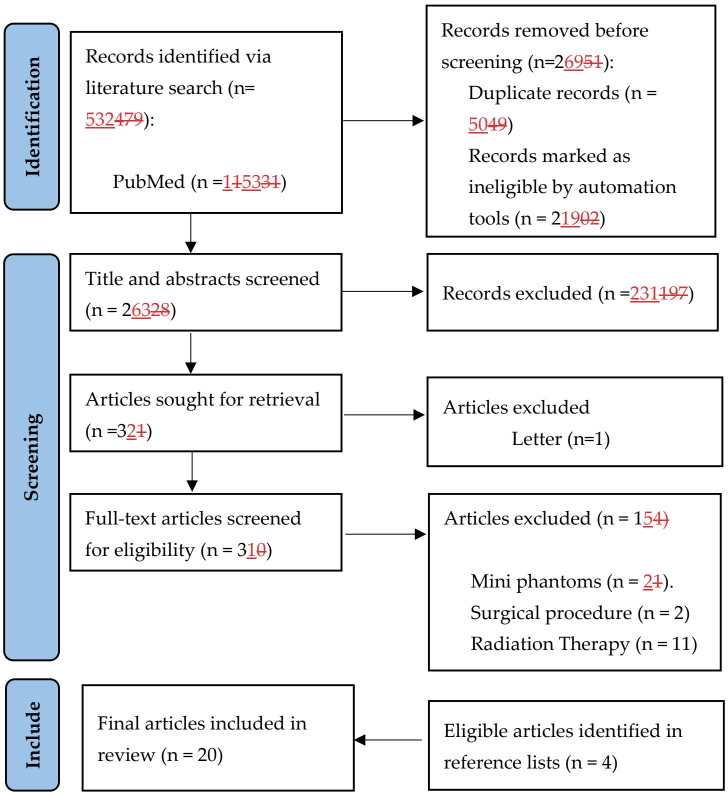

Formatted: Font color: Auto

Formatted: Font color: Auto

Figure 1. PRISMA diagram showing search strategy to identify eligible studies.

2.4 Data Extraction and Synthesis

Studies were summarised according to their purpose and applications for printing the 3D thoracic phantoms, organs fabricated, number of pulmonary nodules, 3D printing method, printers, materials used, relevant findings and country where the studies were conducted (Table 1). Additionally, radiation attenuations were recorded for the different materials and according to thoracic structure produced (Table 2, Figure 2~~3~~).

3. Results

~~Four hundred and seventy-nine~~Five hundred and thirty-two studies were initially retrieved and after review, 20 studies met the selection criteria for inclusion in the analysis as demonstrated in Figure 1. Table 1 lists the study characteristics of these 20 studies from year of publication to study design and key findings.

Article	Year	Study Purpose	Country of Origin	Organs	3DPM /Modelling Segmentation Software/Printer Costs and Time	3D Printing Materials	Lesions	Key Findings and Limitations
[3020]	2018	Low-cost cardiac phantom for optimising cardiac CT protocols.	Australia	Heart	FDM 3D Slicer Creatbot DM Plus $70US 12.1hrs	ABS Contrast (aorta) Oil (fat) Jelly (muscle)	0	A low-cost radiation equivalent, commercial phantom derived with filling materials having similar CT attenuation value to those of the real patient's images. Aorta, fat, and muscle had HU differences of 8%, -3% and 5% relative to patient, respectively, representing a maximum error up to 27HU. The phantom lacks haemodynamic flow and was not developed from real patient's images. Testing scanning protocols was not investigated.
[3121]	2019	Pulmonary artery phantom with simulated embolism for optimising CTPA protocols.	Australia	Pulmonary trunk and arteries	SLS AnalyzeDirect Printer N/P Costs N/P Time N/P	Elastoplastic	2 pulmonary emboli	Geometrically accurate, optimised protocols for PE detection with dose reduction by up to 80%, lacked HU equivalence test, static rather than dynamic representing blood flow.
[3222]	2023	Feasibility of low-cost thoracic phantom for CT reproducibility assessments. Proposed application for CT quality assurance and dose optimisation.	USA	Lung, Fat, Muscle, Bones, vessels, nodules	FDM inPrint, Materialise Ultimaker 5S 270€ ($450AUD) 3 days	PLA at varied infills	1	Comprehensive thoracic model, not radiation and geometrically equivalent. Bone, fat, muscle, lung, vessels, and lesions had HU differences of -69%, -903%, -1772%, -7%, -319% and- 75% relative to patient, respectively. Representing a maximum HU error of up to 505HU. Although PLA is a widely popular material, there was a lack of systematic assessment of recent materials with mixed metallic additives for better HU replication.
[3323]	2023	Low-cost patient-specific lung tumour phantoms for imaging algorithm validation.	Austria	Lung tumours	FDM Materialize Mimics Original Prusa i3 MK3S Costs N/P Time N/P	PLA, ASA, PETG, Nylon at varied infills.	12 (6 different samples of 2 tumours)	Homogenous and heterogeneous tumours created with varied infills between central and peripheral aspects. Good radiation equivalence, achieving average attenuations between -100 and 100HU, consistent with the 17 patient samples. Adequate geometrical agreement of 97% for the 6 lesion samples and 78% for the smaller 6 lesion samples. Smaller lesions were less geometrically accurate due to spatial resolution limitations of the printer.
[3424]	2022	Feasibility of CT-derived skeletal thorax phantom with realistic heterogeneous cortical and spongy bone attenuation. Proposed application for validation of CT procedures.	Austria	Ribs, vertebral column, soft tissue	FDM Materialize Mimics Original Prusa i3 MK3S Costs N/P Time N/P	StoneFill PLA at varied infills and perimeters.	0	Radiation equivalence of heterogeneous bone was achieved (-482 to 968 HU) with a single print material, facilitating a simple fabrication process. HU differences of -9.8%, -150%, -7.5% and -9.4% for the cancellous bone of the dorsal vertebral column, vertebral body, ribs and soft tissue respectively, representing a maximum error up to 30HU by varying infill. Cortical bone matched patient attenuations (230-910HU) by varying number of perimeters.
[3525]	2020	Feasibility of CT-derived skeletal thorax phantom with morphological and radiological accuracy. Proposed applications include exposure optimisation, medical education, skills practice, and surgical guidance.	Austria	Ribs, vertebral column	PolyJet Materialize Mimics Connex3 Objet500 Costs: N/P 120hrs printing, ≥12 days production	Bone meal powder, epoxy and polypropylene amalgamate injected into rigid Vero pure white mold, flexible Agilus30 Clear (FLX935) for encapsulating the skeletal integument. SUP706B support material	0	Reproduced average HU accurately. Dorsal vertebral column, vertebral bodies and ribs had a 1.6%, -8.8%, and -3% HU difference between that of the patient, respectively, with a maximum HU error of 19HU. Lacked heterogeneous bone composition, unable to achieve above 705HU, 85% geometrical overlap - physical discrepancy between structures due to printing in separate parts.
[3626]	2018	Feasibility of creating a thorax phantom based on patient with lung cancer for Xray quality analysis.	Netherlands	Ribs, vertebral column, scapulae, soft-tissue, Lung surface,	Binder Jetting and SLS Zcorp 650 and EOS GmbH Materialize Mimics	Gypsum (bone) Nylon (tumours, lung structures),	3	HUs varied from patient, with lower lung and higher bone/soft tissue values. HU differences between patient and phantom were 124 %, 49%, -26%, and -28.6%

Article	Year	Study Purpose	Country of Origin	Organs	3DPM /Modelling Segmentation Software/Printer Costs and Time	3D Printing Materials	Lesions	Key Findings and Limitations
		Proposed for protocol optimisation and software validation.		airways, lung blood vessels, nodules	US$3,500 Time N/P	Silicon Dragon Skin (cast for soft tissue).		for soft tissue, bone, lung structures and lesions respectively, giving a HU error up to 221HU. Accurate geometrical comparison to patient image with mean differences <1 mm for all tissues. Multiple printed parts assembled, posed challenge to accuracy of spatial relationships. Lacked aerated lung density.
[3727]	2019	Lung phantom with modelled vessels, used for CT image quality assessment and validating reconstruction methods.	Netherlands	Lung vessels, soft-tissue, vertebral column	MJM ProJet HD 3000 3D Slicer $few hundred Time N/P	Visijet EX200 (vessels), PMMA (soft tissue), Teflon (vertebra)	0	Shape and HUs varied from patients. Lower lung (air representation, lack of parenchyma) and higher vessels, bone, and soft tissue attenuations. Marked HU differences of 2000%, 11.43%, 271.88%, and 352.38% compared to patient for vessels, lung interstitium, soft tissue and vertebra respectively, giving an error up to 99HU. MultiJet printing is expensive, despite allowing high level of detail and smooth surfaces.
[3828]	2020	Patient-specific chest phantoms with lesions. Proposed for validating quantitative CT software, calibrating CT intensity (quality assurance), education.	South Korea	Right lung lobe, airway, lesions	FDM DP200, Shindoh Co and Ultimaker 3 Materialize Mimics Cost N/P Time N/P	ABS, TPU (different infills)	N/P	Lung parenchyma of ABS (-705 ±108HU) and TPU phantoms (-630±62HU) was within range of patient attenuations (-600 to -900HU). Solid nodules differed to patient by 31% and 86% for ABS and TPU phantoms respectively, an error up to 85HU. Added artificial lesions. Bone ignored due to higher HU requirements. Tissue texture was unnatural due to laminae from successively layering material.
[3929]	2023	Patient-specific chest phantom with lesions of realistic HU proposed for validating quantitative CT software, CT intensity calibration, educational purposes and patient communication.	South Korea	Lung lobes, lesions, spine, ribs, heart, muscle, skin, fat	FDM Stratasys Fortus 900MC and Ultimaker S5 Materialize Mimics Cost N/P Time N/P	Flexible TPU (heart), hydrophilic PLA + contrast (bone), Cast: Silicone (FlexFoam-iT! Series, Lesions), Gel wax (fat), Ecoflex0020 silicone (muscle), Silicon Dragon (Skin)	6	Comprehensive thoracic model, HU was within range of normal values for all structures except bone (200HU instead of >1000HU) as the contrast was not well absorbed. Attenuation differences between patient and phantom for muscle, fat, skin and solid nodules were 0%, -39% 36% and 19% respectively. Accurate dimensions within 0.2 ± 0.18 mm. Lesions fabricated and randomly placed, rather than based off real patient data. Axial slice rather than entire torso.
[4030]	2023	Reproduce an axial slice of a commercial thorax phantom, proposed for optimising radiation exposures for specific patient groups that are not adequately represented by commercial phantoms (pregnant woman, overweight individuals).	Germany	Lung, Muscle, Breast tissue, bone and cartilage	FDM industrial MEX printer (3ntr A2 V4; 3ntr, Oleggio, Italy-multi-material) 3D Slicer 39€ (64 AUD – exclude printer) 58hrs	PLA (infill: 95% muscle, 30% lung), Granite-PLA (bone), PETG (Cartilage), ABS (breast adipose), PMMA (glandular breast)	0	Commercial phantom derived rather than based off real patient. Similar HU achieved to commercial phantom, except bone was 160HU lower, and lung 110HU higher. All tissues in-range of human norms. Doesn't differentiate between muscle and fat layers. Slight geometrical differences: post-polymerisation shrinkage of ABS and lengthening due to segmentation errors. Multi-material printer allowing 3 different materials to be printed in one step is expensive and not widely available. Phantom fails to distinguish between cortical bone, cancellous bone, and bone marrow.
[4131]	2020	Patient-derived low-cost paediatric torso phantom from only 2 materials, for CT imaging assessment and dosimetry purposes.	USA	Lung, Soft tissue, heart, oesophagus, ribs, clavicles, scapula, vertebral column	FDM Ultimaker 3 (dual extrusion) 3D Slicer $160US 1week/~120hrs	PLA (soft tissues and others), PLA-Fe (bones) at different infills	0	Very similar HU to patient with an error of 100-200HU for soft tissue and bone respectively. Strong linear correlation between infill density and CT number. Automated process printed in one build without need for post-processing and backfilling. Only a 10cm axial cross section reproduced. Doesn't differentiate between muscle, fat, and skin soft tissue layers.
[184]	2022	Patient-specific 3D printed coronary artery model for CTPA optimisation.	Denmark	Coronary arteries	FDM Invesalius 3 Dimension Elite €43 7hrs	Platinum curved silicone rubber (Ecoflex 00-35) + Visipaque contrast + gelatine + NaCl	0	Coronary artery model demonstrated accurate radiation equivalence, within 15% of patient HU's. Protocols with ASiR-V above 60% were non-diagnostic. Imbedded in an expensive commercial phantom and with a porcine heart, not true to patient.

Article	Year	Study Purpose	Country of Origin	Organs	3DPM /Modelling Segmentation Software/Printer Costs and Time	3D Printing Materials	Lesions	Key Findings and Limitations
[4232]	2018	Propose a new method of 3D printing patient chest using PBP variation of filament extrusion amount per unit distance.	Malta	N/P	FDM T-Rex 2 (Formbot) N/A Cost N/P Time N/P	PLA	0	PBP produced significantly wider HU range compared to VID method and more closely resembled patient HU's, however with longer printing times. Morphologically more similar by visual inspection. Converts CT image directly into printer instructions to control extrusion rate per voxel, without intermediate step of segmentation. Phantom dimensions and tissues included is undescribed. High enough bone attenuation was not achieved. Different scanner and parameters used for patient and phantoms may explain different HU.
[4333]	2023	PixelPrint method to print COVID-19 lung phantoms by modifying printer-head speed, with constant filament extrusion rate. Proposed for validation of algorithms and protocol optimisation.	USA	N/P	FDM Lulzbot TAZ 6 N/A Cost N/P Time N/P	PLA	0	Converts CT image directly into printer instructions to control the printhead speed per voxel, without intermediate step of segmentation. Subjective radiologist assessment determined that there were non-clinically significant differences (mean score difference: 0.03-0.29) between real patient and phantom slices in terms of diagnostic confidence, image contrast and image noise (p<0.0005, effect size = 0.03-0.31), as well as resolution (p>0.05) on a scoring scale of 1-5.
[4434]	2022	Evaluation of PixelPrint method to print COVID-19 lung phantoms of different severity with accurate geometry, texture, and attenuation profiles. Proposed for protocol optimisation, CT research and ground-truths for radiomics.	USA	Lung (parenchyma and vessels).	FDM Lulzbot TAZ 6 N/A Cost N/P 24 hrs	PLA	0	Phantom attenuations were achieved by different volumes of filament per voxel. Mean HU differences between patient and phantom for lung parenchyma and vessels were within 15HU. Geometrically equivalent within printer resolution error. Strong radiomics correlation of contrast and texture between patient and phantom images (r >0.95).
[4535]	2023	Compare the detection sensitivity of paediatric lung nodules using different image reconstruction methods.	South Korea	Lung Nodules	SLA RS pro-800 TeraRecon 3D program Cost N/P Time N/P	PLA	3	Determined that the fast non-local means filter is better than iterative reconstruction at reducing image noise whilst preserving contrast and sharpness for better lung nodule detection. Printed the irregular shape of the nodules extracted from real patient data, however, lacked formal morphological and geometrical analysis. Nodules did not reflect the various attenuations of the patients' nodules (-37-665HU), however, was within range (145-185HU). Lacked vessels and parenchyma. Embedded into an expensive commercial phantom.
[4636]	2022	Feasibility of using low-density paper and inkjet-printing to simulate diseased lung parenchyma and lung nodules as ground truths for radiomics. Proposed for application of CT protocol optimisation and software validation.	USA	Lung parenchyma and nodules	Inkjet Printing HP Deskjet 6940 ITK-SNAP Cost N/P Time N/P	Kimtech Science Wipes with potassium iodide solution	1	Phantom slices achieved good Pearson correlation of attenuations compared to patient slices (r =0.83-0.92). Lung parenchyma (-830-200HU) was unable to re-create near air densities <-1000HU due to limitations of paper substrate. Radiomic comparisons showed a median absolute difference of 6.1% and good morphological consensus with shaped features demonstrating <25% difference.
[4737]	2021	Aortic dissection phantom with TEVAR stent in-situ for optimising routine follow-up CTA protocols.	Switzerland	Aorta	PolyJet Printer: N/P 3D Slicer Cost N/P Time N/P	Visijet CE-NT, Agilus,	0	A patient-specific aortic dissection 3D printed model with a TEVAR stent was developed, having similar material and radiological properties to humans. Dose reduction of at least 20% enabled by reducing kVp from 120 to 80, whilst maintaining diagnostic image

Article	Year	Study Purpose	Country of Origin	Organs	3DPM /Modelling Segmentation Software/Printer Costs and Time	3D Printing Materials	Lesions	Key Findings and Limitations
								quality. Lacked haemodynamic flow and realistic surrounding tissue environment.
[4838]	2019	Development of a cost-effective personalised chest phantom, proposed for dose optimisation.	China	Skin, fat, muscle, lung, lesion, ribs, scapula, sternal angle	Method: N/P Printer: N/P, photosensitive printer Materialise Mimics Cost: N/P Time: N/P	ABS (skin shell), Molted M3 wax + $CaCO_3$ + MgO (Fat), ABS-Bismuth (bones), water, agarose, NaCl + pearl powder (Muscle and lesions), foamed silica gel (lung).	1	A patient-specific chest phantom consisting of a 3D printed skin and fat shell with filling materials, similar in morphology and radiation attenuation properties to the real CT. HU differences of 25%, 30%, 20% and 35% between patient and phantom for fat, muscle, bone, and tumour respectively. This represents a 20HU difference for fat, muscle, and lesion and 55HU difference on average for bone. Lacked geometrical analysis as well as HU analysis for lung tissue and skin.

Abbreviations -3DPM: three-dimensional-printing method, PE: Phantom Experiment, N/P: Not provided, 3DP: three-dimensional-printing, CT: Computed Tomography, CTPA: CT Pulmonary Angiography, FDM: Fused Deposition Modelling, SLS: Selective Laser Sintering, MJM: Multi-Jet Modelling, PLA: Polylactic acid, ABS: acrylonitrile butadiene styrene, TPU: thermoplastic polyurethane, MEX: Material Extrusion, PETG: Polyethylene terephthalate glycol, PMMA: polymethyl methacrylate, PLA-FE: magnetic iron PLA (composite of iron powder and PLA), PBP: pixel by pixel, N/A: not applicable, PE: Pulmonary embolism, SLA: Stereolithography or Stereo lithography appearance, TEVAR: Thoracic endovascular aortic repair., ASA: acrylonitrile styrene acrylate, ASiR-V: adaptive statistical iterative reconstruction-V.

Table 2. Hounsfield Units (HU) achieved for different thoracic tissues.

Article	Scanner	Parameters	Skin	Fat	Muscle	Soft tissue combined	Vessels	Bone	Lung Parenchyma	Lung Nodules	Airways	Heart	Breast
[3020]	Alexion, ToshibaAlexion, Toshiba Medical Systems Co Ltd., Otowara, Japan)	120kVp, 200mA	-	Oil -92.4HU	Jelly 25.9 HU	-	Contrast 354.3 HU	-	-	-	-	-	-
[3222]	Siemens Somatom Force (Siemens Healthineers, Erlangen, Germany)	120kVp, 50mAs	-	PLA (40% infill) −657 ± 55.46 HU	PLA (55% infill) −469 ± 79.16HU	-	PLA (70% infill) −295 ± 43.93 HU	PLA (100% infill) −132.16 ± 103.66 HU	PLA (10% infill) −933.17 ± 63.89 HU	PLA (62.5% infill) −357 ± 56.12HU	-	-	-

Formatted: Font color: Auto

Formatted: Font color: Auto

Table 2. Hounsfield Units (HU) achieved for different thoracic tissues.

Article	Scanner	Parameters	Skin	Fat	Muscle	Soft tissue combined	Vessels	Bone	Lung Parenchyma	Lung Nodules	Airways	Heart	Breast
[3323]	SOMATOM Definition AS, Siemens Healthineers, GermanySyngo CT VA40A, Siemens Healthineers	120kVp, 200mAs	-	-	-	-	-	-	-	ASA (100%) 155HU, 30HU (97%), PLA: -75 HU (82% infill), 10 HU (91% Infill), Nylon: 54HU (100%), -75HU (94%), PETG: 227 (100%), 47 (85%)	-	-	-
[3424]	SOMATOM Definition AS, Siemens Healthineers. Erlangen Germany,	120kVp, 315 mAs	-	-	-	-	-	StoneFill PLA (30-100% Infill) =-482 to 968HU	-	-	-	-	-
[3525]	SOMATOM Definition AS, Siemens Healthineers. Erlangen Germany,	120kVp, 315 mAs	-	-	-	-	-	Bone meal powder, epoxy, polypropylene = 42-705HU	-	-	-	-	-
[3626]	GE Discovery CT590	120 kVp	-	-	-	Silicone Dragon Skin -168 to 95HU (μ=-43HU)	Nylon = -779 to -229 (μ=-512 HU)	Gypsum= 372-995HU (μ = 731)	Nylon = -779 to -229 (μ=-512 HU)	Nylon =-632 to 50 HU (μ=-130HU)	Nylon = -779 to -229 (μ= -512 HU)	-	-
[3727]	Toshiba Aquilion Genesis	120 kVp, Sure Exposure	-	-	-	PMMA 119 ± 10 HU	Visijet Ex200 104 ± 22 HU	Teflon 119 ± 8 HU	Air −985 ± 18 HU	-	-	-	-
[2388]	dual-source CT SOMATOM Definition	120kVp	-	-	-	-	-	-	50% infill: ABS -705 ± 108 HU,	90% Infill: ABS 68 ± 16HU TPU 15 ± 18HU	-	-	-

Formatted: Font color: Auto

Formatted: Font color: Auto

Formatted: Font color: Auto

Formatted: Font color: Auto

Formatted: Font color: Auto

Formatted: Font color: Auto

Table 2. Hounsfield Units (HU) achieved for different thoracic tissues.

Article	Scanner	Parameters	Skin	Fat	Muscle	Soft tissue combined	Vessels	Bone	Lung Parenchyma	Lung Nodules	Airways	Heart	Breast
	Flash, Siemens								TPU -630 ± 62HU				
[3929]	dual-source CT SOMATOM Definition Flash, Siemens	120kVp	Silicone Dragon Skin Fx Pro 165 ± 29HU	Gel wax -160 ± 21HU	Silicone ExoFlex 0200 111 ± 23HU	-	-	Hydrophilic PLA + contrast 200 ± 24HU	Silicone FlexFoam-iT! 17 -651 ± 16HU	FlexFoam-iT! V:-909 ±18HU, FlexFoam-iT! 23FR: -683 ± 23HU	-	Flexible TPU N/A	-
[4030]	GE Bright Speed Bright Speed; General Electrics, Boston,Massachusetts, USA	120 kVp, 200mA, 0.8s	-	-	PLA (95% Infill): 35 ± 25HU	-	-	Granite PLA composite filament 700 ± 50HU	PLA (30%) -690 ± 80HU	-	-	-	ABS (adipose) -30±10HU PMMA (glandular) 95±15HU
[4131]	Siemens Biograph mCT	120kVp, 250mAs	-	-	-	PLA (94 %) 31 ± 79 HU	-	PLA-Fe (50%) 1180 ± 1107 HU	PLA (46%) −417 ± 434 HU	-	-	PLA, 94 ± 46HU	-
[181]	GE Revolution GE healthcare Waukesha, WI, USA	100kVp, 50-570 mA	-	-	-	-	Ecoflex, contrast, 318 ± 4 HU	-	-	-	-	-	-
[4232]	Phillips, Brilliance 64	120kVp, 339mA	-	-	PLA 32 HU	-	PLA 139HU	PLA 153HU	PLA -570HU	-	-	-	-
[4434]	GE Revolution, Siemens Sensation-64	Not mentioned	-	-	-	-	PLA -3.9 ± 18.6 HU	-	PLA -771 ± 34 HU	-	-	-	-
[4535]	SOMATOM Definition AS, Siemens Healthineers.	80 and 100kVp	-	-	-	-	-	-	-	PLA 145-185HU	-	-	-
[4636]	Siemens Somatom Force	120kVp, 200mAs	-	-	-	-	-	-	Kimtech Science Wipes + KI -830-200HU	Kimtech Science Wipes + KI N/A	-	-	-

Formatted: Font color: Auto

Formatted: Font color: Auto

Formatted: Font color: Auto

Formatted: Font color: Auto

Formatted: Font color: Auto

Formatted: Font color: Auto

Formatted: Font color: Auto

Formatted: Font color: Auto

Table 2. Hounsfield Units (HU) achieved for different thoracic tissues.

Article	Scanner	Parameters	Skin	Fat	Muscle	Soft tissue combined	Vessels	Bone	Lung Parenchyma	Lung Nodules	Airways	Heart	Breast
[4737]	Siemens Somatom Force	120 kVp 150 mAs	-	-	-	-	Visijet CE-NT 90.6 HU	-	-	-	-	-	-
[4838]	Phllips, Brilliance 256	120kVp, 260mAs	ABS N/A	Molted M3 wax, $CaCO_3$, MgO, -100 to -60HU	Water, NaCl, Agarose, pearl powder, 20-60HU	-	-	ABS + Bismuth 120-300HU	Foamed silica gel N/A	Water, NaCl, Agarose, pearl powder 17-49HU	-	-	-

Abbreviations – HU: Hounsfield Units, μ: mean, PLA: Polylactic Acid, TPU: thermoplastic polyurethane, ABS: Acrylonitrile Butadiene Styrene, PMMA: Poly(methyl methacrylate, N/A: not assessed, KI : Potassium Iodide, $CaCO_3$: Calcium Carbonate, MgO : Magnesium Oxide, NaCl : Sodium Chloride, PETG: Polyethylene terephthalate glycol

Formatted: Font color: Auto

Formatted: Font color: Auto

Formatted: Font: 7 pt

Formatted: Subscript

applied sciences

MDPI

Figure 2. Range of materials with radiation attenuations (HU) representing different thoracic structures.

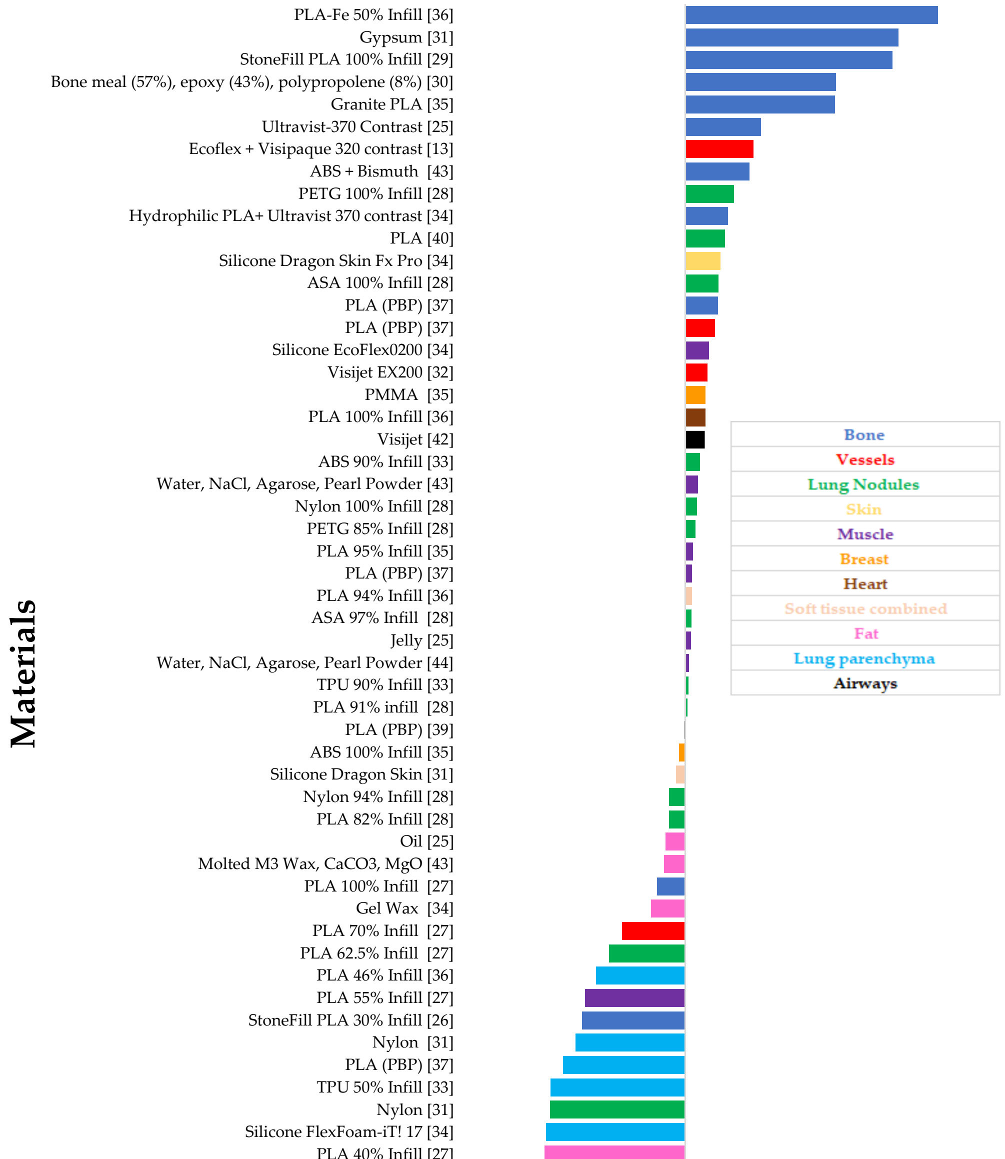

Figure 2. Range of materials with radiation attenuations (HU) representing different thoracic structures.

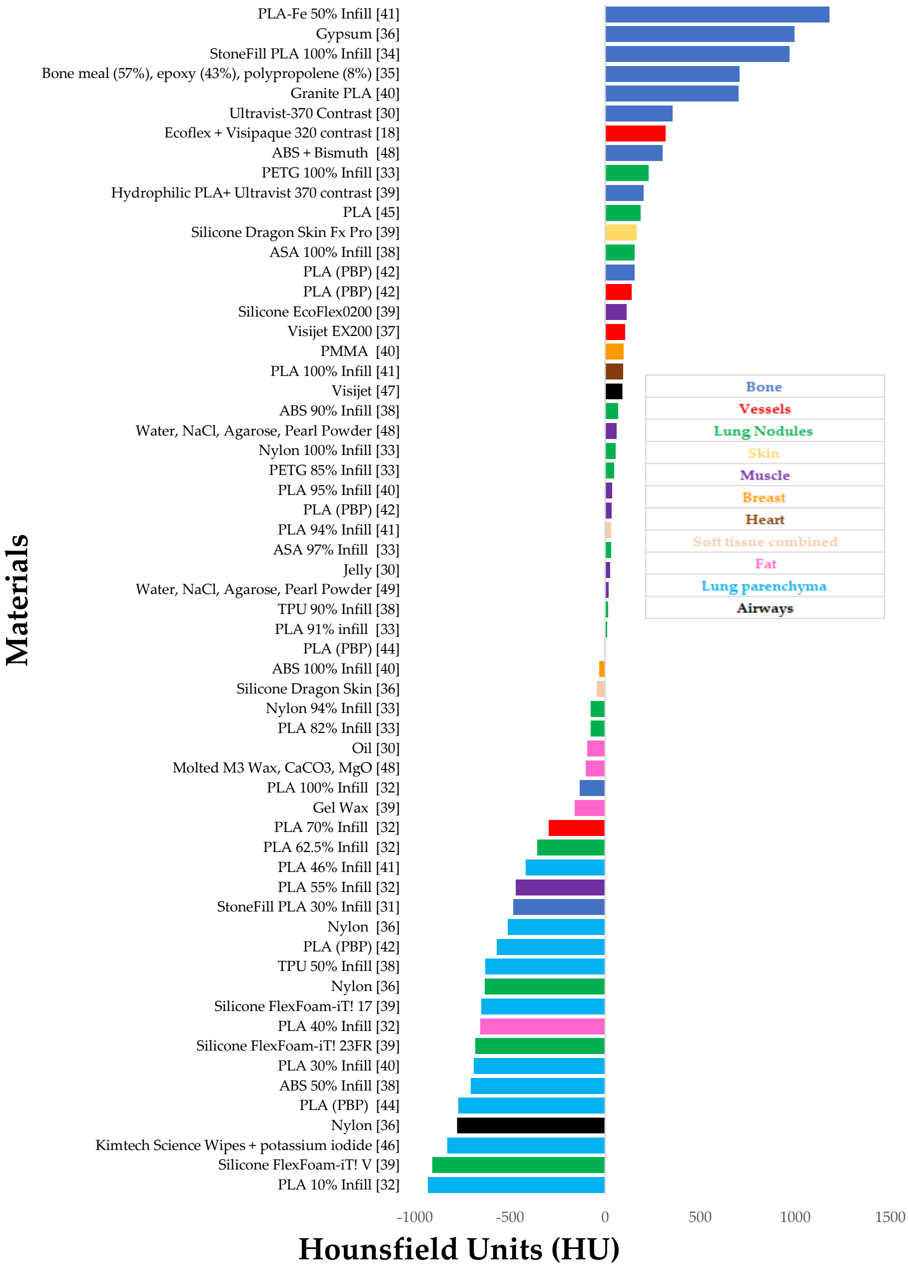

applied sciences

MDPI

215

Table 3. Quality assessment scores according to the Crowe Critical Appraisal Tool (CCAT) v1.4

Article	Preliminaries	Introduction	Design	Data Collection	Ethics/Conflicts of Interest	Results	Discussion	Total
[20]	4	4	5	2	4	4	3	26/35 (74%)
[21]	4	5	4	3	5	4	4	29/35 (83%)
[22]	4	5	4	3	5	2	3	27/35 (77%)
[23]	4	5	3	2	5	4	5	27/35 (77%)
[24]	5	5	3	3	5	3	3	26/35 (74%)
[25]	5	5	3	2	5	4	3	27/35 (77%)
[26]	5	5	4	3	4	3	5	30/35 (86%)
[27]	5	4	4	4	3	2	4	26/35 (74%)
[28]	4	3	4	4	4	2	3	24/35 (69%)
[29]	5	4	4	2	5	2	4	26/35 (74%)
[30]	4	5	4	3	4	3	4	27/35 (77%)
[31]	4	5	4	4	5	3	4	29/35 (83%)
[11]	4	5	3	3	4	3	4	25/35 (71%)
[32]	3	4	2	3	4	2	4	23/35 (66%)
[33]	4	5	3	5	4	3	5	29/35 (83%)
[34]	3	2	2	3	4	2	1	17/35 (49%)
[35]	4	4	3	2	3	3	3	20/35 (57%)
[36]	5	4	2	2	5	2	4	24/35 (69%)
[37]	5	5	3	4	5	3	5	30/35 (86%)
[38]	5	5	4	2	5	2	3	26/35 (74%)

216

Formatted: Tab stops: 2.95 cm, Left

~~Articles were scored using a scale from 0-5, with 0 indicating unacceptable, 1-2 indicating poor, 3 indicating moderate, 4 good and 5 excellent according to the criteria described by~~

Table 3. Quality assessment scores according to the Crowe Critical Appraisal Tool (CCAT) v1.4

Article	Preliminaries	Introduction	Design	Data Collection	Ethics/Conflicts of Interest	Results	Discussion	Total
[30]	4	4	5	2	4	4	3	26/35 (74%)
[31]	4	5	4	3	5	4	4	29/35 (83%)
[32]	4	5	4	3	5	3	3	27/35 (77%)
[33]	4	5	3	3	5	2	5	27/35 (77%)
[34]	5	5	3	3	5	2	3	26/35 (74%)
[35]	5	5	3	2	5	4	3	27/35 (77%)
[36]	5	5	4	3	5	3	5	30/35 (86%)
[37]	5	5	4	4	2	2	5	27/35 (77%)
[38]	5	2	4	4	4	2	3	24/35 (69%)
[39]	5	4	4	2	5	2	4	26/35 (74%)
[40]	4	5	4	3	4	3	4	27/35 (77%)
[41]	4	5	4	4	5	3	4	29/35 (83%)
[18]	4	5	3	3	4	2	4	25/35 (71%)
[42]	3	4	3	3	4	2	4	23/35 (66%)
[43]	4	5	3	5	4	3	5	29/35 (83%)
[44]	3	2	2	3	4	2	1	17/35 (49%)
[45]	4	4	3	2	2	2	3	20/35 (57%)
[46]	5	4	2	3	2	2	4	22/35 (63%)
[47]	5	5	3	4	5	3	5	30/35 (86%)
[48]	5	5	4	2	5	2	3	26/35 (74%)

Articles were scored using a scale from 0-5, with 0 indicating unacceptable, 1-2 indicating poor, 3 indicating moderate, 4 good and 5 excellent according to the criteria described by Crowe, Sheppard and Campbell [29~~19~~]. The scores were summed, giving a total quality indicator ranging from 0-20% which was considered inadequate, 20-50%: poor, 50-60%: moderate, 60-80%: good and 80-100%: excellent quality.

Formatted: Font color: Auto
Formatted: Font color: Auto
Formatted: Font color: Auto
Formatted: Font color: Auto
Formatted: Font color: Auto
Formatted: Font color: Auto
Formatted: Font color: Auto
Formatted: Font color: Auto
Formatted: Font color: Auto
Formatted: Font color: Auto
Formatted: Font color: Auto
Formatted: Font color: Auto
Formatted: Font color: Auto
Formatted: Font color: Auto
Formatted: Font color: Auto
Formatted: Font color: Auto
Formatted: Font color: Auto
Formatted: Font color: Auto
Formatted: Font color: Auto
Formatted: Font color: Auto
Formatted: Font color: Auto

applied sciences

MDPI

Category Item	Description of item [☑ Present; ☒ Absent; ■ Not applicable]	Score [0–5]
Preamble		
Text	1. Sufficient detail others could reproduce ❑ 2. Clear/concise writing ❑, table(s) ❑, diagram(s) ❑, figure(s) ❑	**Preamble score**
Title	1. Includes study aims ❑ and design ❑	
Abstract	1. Key information ❑ 2. Balanced ❑ and informative ❑	
Introduction		
Background	1. Summary of current knowledge ❑ 2. Specific problem(s) addressed ❑ and reason(s) for addressing ❑	**Introduction score**
Objective	1. Primary objective(s), hypothesis(es), or aim(s) ❑ 2. Secondary question(s) ❑	
Design		
Research design	1. Research design(s) chosen ❑ and why ❑ 2. Suitability of research design(s) ❑	**Design score**
Intervention, Treatment, Exposure	1. Intervention(s)/treatment(s)/exposure(s) chosen ❑ and why ❑ 2. Precise details of the intervention(s)/treatment(s)/exposure(s) ❑ for each group ❑ 3. Intervention(s)/treatment(s)/exposure(s) valid ❑ and reliable ❑	
Outcome, Output, Predictor, Measure	1. Outcome(s)/output(s)/predictor(s)/measure(s) chosen ❑ and why ❑ 2. Clearly define outcome(s)/output(s)/predictor(s)/measure(s) ❑ 3. Outcome(s)/output(s)/predictor(s)/measure(s) valid ❑ and reliable ❑	
Bias, etc	1. Potential bias ❑, confounding variables ❑, effect modifiers ❑, interactions ❑ 2. Sequence generation ❑, group allocation ❑, group balance ❑, and by whom ❑ 3. Equivalent treatment of participants/cases/groups ❑	
Sampling		
Sampling method	1. Sampling method(s) chosen ❑ and why ❑ 2. Suitability of sampling method ❑	**Sampling score**
Sample size	1. Sample size ❑, how chosen ❑, and why ❑ 2. Suitability of sample size ❑	
Sampling protocol	1. Target/actual/sample population(s): description ❑ and suitability ❑ 2. Participants/cases/groups: inclusion ❑ and exclusion ❑ criteria 3. Recruitment of participants/cases/groups ❑	
Data collection		
Collection method	1. Collection method(s) chosen ❑ and why ❑ 2. Suitability of collection method(s) ❑	**Data collection score**
Collection protocol	1. Include date(s) ❑, location(s) ❑, setting(s) ❑, personnel ❑, materials ❑, processes ❑ 2. Method(s) to ensure/enhance quality of measurement/instrumentation ❑ 3. Manage non-participation ❑, withdrawal ❑, incomplete/lost data ❑	
Ethical matters		
Participant ethics	1. Informed consent ❑, equity ❑ 2. Privacy ❑, confidentiality/anonymity ❑	**Ethical matters score**
Researcher ethics	1. Ethical approval ❑, funding ❑, conflict(s) of interest ❑ 2. Subjectivities ❑, relationship(s) with participants/cases ❑	
Results		
Analysis, Integration, Interpretation method	1. A.I.I. method(s) for primary outcome(s)/output(s)/predictor(s) chosen ❑ and why ❑ 2. Additional A.I.I. methods (e.g. subgroup analysis) chosen ❑ and why ❑ 3. Suitability of analysis/integration/interpretation method(s) ❑	**Results score**
Essential analysis	1. Flow of participants/cases/groups through each stage of research ❑ 2. Demographic and other characteristics of participants/cases/groups ❑ 3. Analyse raw data ❑, response rate ❑, non-participation/withdrawal/incomplete/lost data ❑	
Outcome, Output, Predictor analysis	1. Summary of results ❑ and precision ❑ for each outcome/output/predictor/measure 2. Consideration of benefits/harms ❑, unexpected results ❑, problems/failures ❑ 3. Description of outlying data (e.g. diverse cases, adverse effects, minor themes) ❑	
Discussion		
Interpretation	1. Interpretation of results in the context of current evidence ❑ and objectives ❑ 2. Draw inferences consistent with the strength of the data ❑ 3. Consideration of alternative explanations for observed results ❑ 4. Account for bias ❑, confounding/effect modifiers/interactions/imprecision ❑	**Discussion score**
Generalisation	1. Consideration of overall practical usefulness of the study ❑ 2. Description of generalisability (external validity) of the study ❑	
Concluding remarks	1. Highlight study's particular strengths ❑ 2. Suggest steps that may improve future results (e.g. limitations) ❑ 3. Suggest further studies ❑	

Formatted: Centered

Figure 3. Critical Appraisal tool used to determine quality of studies [29]. Reprinted with permission from Crowe et al. [29]. Note: one assessor rated the quality of studies according to this appraisal tool. Sampling section was removed due to the nature of study designs being single phantom experiments.

Formatted: Font: 9 pt, Bold, Not Italic, English (Australia)

Formatted: Font: 9 pt, Not Italic, English (Australia)

Formatted: Font: 9 pt, Not Italic, Font color: Auto, English (Australia)

Formatted: Font: Not Italic, Font color: Auto

Formatted: Font: 9 pt, Not Italic, Font color: Auto, English (Australia)

Formatted: Font: Not Italic, Font color: Auto

Formatted: Font: 9 pt, Not Italic, Font color: Auto, English (Australia)

Formatted: Font: 9 pt, Not Italic, English (Australia)

Formatted: MDPI_2.2_heading2, Space Before: 12 pt, Line spacing: Exactly 11 pt, Tab stops: 10.01 cm, Left

Formatted: Font: 9 pt, English (Australia)

Formatted: Normal, Indent: Left: 0 cm, First line: 0 cm, Space Before: 0 pt

applied sciences

MDPI

3.1. 3D printing thoracic organs

Articles were found to print different thoracic structures, such as lungs [3222,3626-4132,4434,4636,4838], nodules [3222,3323,3626,3828,3929,4535,4636,4838], vessels [181,3020,3222,3626,3727,3929,4131,4232,4434,4737], heart [3929,4131], airways [3626], breast [4030], muscles [3020,2322,3929,4030,4232,4838], skin [3929], fat [3020,3222,3929,4838], and bones of the thorax [3222,3424-3727,3929-4232,4838]. Lungs were the most common thoracic organ printed, with 11 articles (55%) modelling them.

3.2. 3D Printing Methods

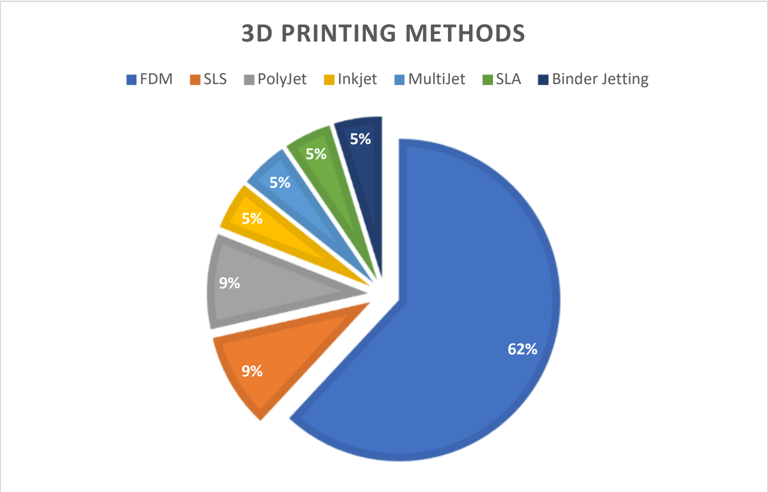

Figure 43. 3D Printing methods for creating chest phantoms. Note: PolyJet differs from MultiJet by having more than one print head, enabling multiple materials in a single print. SLA; stereolithography, FDM; Fused Deposition Modelling. SLS – Selective Laser Sintering. Binder Jetting involves jetting of a liquid adhesive onto a bed of ceramic or gypsum powder [4939].

Figure 3. 3D Printing methods for creating chest phantoms. Note: PolyJet differs from MultiJet by having more than one print head, enabling multiple materials in a single print. SLA; stereolithography, FDM; Fused Deposition Modelling. SLS – Selective Laser Sintering. Binder Jetting involves jetting of a liquid adhesive onto a bed of ceramic or gypsum powder [39].

Fused deposition modelling (FDM) was the most widely applied printing method for developing 3D printed thoracic phantoms reported in the literature [181,3020,3222-3424,3828-4434] (Figure 43).

The range of materials utilised for 3D printed thoracic models and their corresponding radiation attenuations are illustrated in Figure 22. Fifty percent of the studies employed polylactic acid (PLA), making it the most common printing material used [3222-3424,3929-4232,4434,4535]. Studies incorporated high density additives to materials in order to replicate bone structures, including PLA with iron, StoneFill PLA, granite-PLA, ABS with added Bismuth, contrast, and bone meal powder added to polypropylene and epoxy resin. These achieved Hounsfield units ranging between -482 to 1180HU [3222,3424-3727,3929-4232,4838] (Figure 22, table 2). Lower density tissues such as fat and

Formatted: Font color: Auto

Formatted: Font color: Auto

Formatted: Indent: Left: 4.5 cm, First line: 0.85

Formatted: Indent: Left: 0 cm, First line: 0 cm

Formatted: Font color: Auto

Formatted: Font color: Auto

Formatted: Font color: Auto

lung parenchyma were produced with low infill ratios of polymer materials, intrinsically low-density materials including TPU, Nylon and silicone foam as well as low density paper [32~~22~~,46~~36~~,48~~38~~]. Radiation densities ranged from, -160 to -60HU for fat, -469 to 111HU for muscle, and -933 to -417HU for lung parenchyma [32~~22~~,36~~26~~,38~~28~~-42~~32~~,44~~34~~,46~~36~~] (Table 2, Figure 2~~2~~).

3.3. Purposes of 3D printed chest phantoms

Seven out of the 20 studies investigated and assessed the application of 3D printed chest phantoms for specific purposes. This included optimising CT pulmonary angiography protocols [18~~1~~,31~~21~~] and optimising CT angiography (CTA) post thoracic endovascular aortic repair (TEVAR) [47~~37~~]. Four out of these 7 studies utilised the 3D printed thoracic replicas for quality assurance purposes, encompassing CT reproducibility assessments [32~~22~~], X-ray image quality analysis [36~~26~~], validating segmentation and image registration algorithms [33~~23~~] as well as comparing image reconstruction algorithms to enhance detection sensitivity of paediatric lung nodules [45~~35~~].

In contrast, the majority of studies (60%) solely investigated the feasibility of 3D printing for creating radiation-attenuating equivalent thoracic phantoms, without analysing them for direct application [30~~20~~,34~~24~~,35~~25~~,37~~27~~-41~~31~~,43~~33~~,44~~34~~,46~~36~~,48~~38~~]. Despite not directly assessing these applications, studies suggested the utility of their 3D printed thoracic phantoms for optimising CT protocols to reduce dose [30~~20~~,32~~22~~,35~~25~~,36~~26~~,41~~31~~,43~~33~~,44~~34~~,46~~36~~,48~~38~~], evaluating protocols for under-represented groups including infants and pregnant woman [40~~30~~], quality assurance [32~~22~~,37~~27~~-39~~29~~,41~~31~~], validating CT software and procedures [34~~24~~,36~~26~~-39~~29~~,43~~33~~,46~~36~~], serving as ground truths for radiomics [43~~34~~,46~~36~~], for CT research [44~~34~~], as well as supporting anatomy education, surgical guidance and patient comprehension [35~~25~~,38~~28~~,39~~29~~].

3.4. Quality of studies

All 20 eligible studies were phantom experiments of varying quality, ranging from poor (49%) to excellent (86%) quality as assessed by the Crowe Quality Assessment Tool [29~~19~~]. Most studies (n=13) rated good (60-79%) [18~~1~~,30~~20~~,32~~22~~-35~~25~~,37~~27~~-40~~30~~,42~~32~~,46~~36~~,48~~38~~], followed by excellent (80-100%, n=5) [31~~21~~,36~~26~~,41~~31~~,43~~33~~,47~~37~~], with only 1 rating poor [44~~34~~] and 1 as moderate [45~~35~~] (Table 3).

4. Discussion

Analysis of 20 studies included in this review demonstrates several key findings. Firstly, 3D printed phantoms can produce similar morphology and attenuations to human thoracic tissues, on the premise that dedicated material and printing parameters are selected. This offers a promising avenue for precise, cost-effective alternatives to commercially available anthropomorphic phantoms. However, this review reveals that the field of 3D printed thoracic phantoms is in its infancy, with most studies still focused on testing the feasibility of this approach through material experimentation to correlate with tissue-radiodensities, aiming to create radiation-equivalent phantoms [30~~20~~,34~~24~~,35~~25~~,37~~27~~-41~~31~~,43~~33~~,44~~34~~,46~~36~~,48~~38~~]. Few studies have progressed to application stages, having validated radiation equivalence [18~~1~~,45~~35~~,47~~37~~,50~~40~~]. Although, possible applications include using phantoms for quality assurance of medical imaging equipment, optimising imaging protocols, radiomics, software validation, as well as complimenting anatomy education and as practice tools for surgical guidance. Additionally, most studies are single phantom experiments, warranting a broader research base and larger sample size of tho-

Formatted: Font color: Auto

Formatted: Font color: Auto

Formatted: Font color: Auto

Formatted: Font color: Auto

Formatted: Font color: Auto

Formatted: Font color: Auto

Formatted: Font color: Auto

racic phantoms with similar designs tested on a range of patients before clinical implementation can be confidently pursued. Furthermore, phantom results need to be verified against real patients before clinical implementation can be confidently pursued.

4.1 Quality of Studies

Quality of studies were found to be predominantly good, scoring in the 60-79% of the Crowe Quality Assessment bracket. However, most studies scored poorly in their results section, averaging 2/5, demanding further research with stronger methodological rigour. Studies tended to lack statistical analysis to corroborate their findings. For example, most studies claimed radiation equivalence of their phantoms to patients, however, they did not conduct any - any paired sample t teststests to confirm equivalence [1811,3020,3222-3626,3828-4232,4434,4535,4838]. Studies were additionally biased by evaluating their phantom attenuations using different CT scanners and protocols to their patient counterparts 34[24,3626,3727,3929,4232,4535-4737]. Controlling these parameters is paramount as HU values are influenced by different scanners and different voltages [5141]. X-ray attenuation not only depends on the physical density and effective atomic number of the material, but also the energy of the X-ray photons [5242]. Materials with low effective atomic number, such as adipose tissue, exhibit increased Hounsfield Units (HU) with higher energy photons. Conversely, materials with higher effective atomic number, such as bone and calcium, Higher X-ray energies exhibits lower HU with higher energy photons due to thea greater ease in with which the Xray beam penetratesing a giventhem material, diminishing photoelectric absorption, consequently resulting in lower attenuation coefficients (HU) for that material [48,5141,5242]. Appreciably, sourcing the exact scanner poses a practical challenge, given the diverse brands and types available.

Studies were also limited by not detailing phantom costs and printing times. Only 6 studies reported costs, ranging from $64-5500 AUD [181,3020,3222,3727,4030,4131] and 7 studies reported manufacturing time, ranging from 7 hours to 12 days [1811,3020,3222,3525,4030,4131,4434]. Future studies should prioritise transparency by thoroughly documenting their research methodologies, allowing for replication and validation. Although there is limited transparency regarding costs, the reported expenses are notably more affordable than commercial anthropomorphic phantoms, which can reach exorbitant prices upwards of $40, 0000 [5343]. This, coupled with the growing accessibility of 3D printers and printing materials to the general public, makes 3D printed phantoms an attractive option [8].

4.2. 3D printing methods and materials

Most studies printed thoracic models using FDM, involving the additive layering of melted thermoplastics extruded through a heated nozzle onto a printing bed [110]. The popularity of FDM technology can be attributed to the wide availability of commercially available thermoplastic printing materials [8] as well as the growing body of evidence investigating different additives and composite materials in attempts to broaden the profile of radiodensities they can mimic [109,5444,5545]. Furthermore, FDM printers are cheaper and more widely available compared to other printing technologies [2818,5646]. Additionally, FDM enables the manipulation of infill densities: the ratio of printing material lines to air gaps, modifying the density for tailored attenuations [46].

Studies in this review utilised FDM through three primary methodologies: 1. adjusting infill ratios to tailor radiodensities for specific tissue types [3222-3424,3828-4131], 2. Modifying the volume of extruded filament and adjusting extrusion rates per voxel [4232-4434], and 3. crafting skin and external organ shells to encase filler materials of dedicated densities [1811,3020]. Manipulating the infill ratio is advantageous because it allows for the use of fewer material types. Some studies opt for a single material, simplifying the process and reducing costs [3222,3424,4131]. However, this challenged the achievement of radiation equivalence, requiring higher atomic additives for better HU replication [3222]. The pixel-by-pixel method introduces a unique approach to 3D printing by removing the requirement to segment DICOM images [4232,4434]. Instead, CT intensities are directly translated into G-code representing printer instructions of varying extrusion volumes or speeds, allowing for heterogenous densities, with a wider range of attenuations [4232-4434]. Regardless, printing times were longer for the pixel-by-pixel method, and the G-code is proprietary, with one study demonstrating poor methodological quality [4434]. This was due to absence of statistical analysis, lack of detailed information including costs and scanning parameters, measurement bias involving a single assessor, and concluding statements that extended beyond the scope of the study (Table 3). However, the direct conversion from DICOM image to printer instructions likely improves spatial resolution, due to avoiding the subjective contouring and inaccuracies of manual thresholding during segmentation and associated partial volume effects [5747,5848].

_FDM was critiqued by the literature for causing spatial mismatches between patient and phantom replicas because of post-polymerisation shrinkage and small build platforms requiring assembly of printed parts [3525,3626,4030]. This is an already established drawback of FDM polymer materials whereby warping and cracking of the material accrues after cooling, leading to rough surface finishes [8]. Potential oozing of heated remnant material from the nozzle onto the printed surface can exacerbate geometrical errors [4232]. Moreover, FDM applies thicker layers of printed material, resulting in a z-axis resolution typically ranging between 0.1-0.5mm [4939] which can produce stair-step deformities [3828,5949]. Consequently, FDM printers exhibit lower resolution compared to other printing methods, such as Material Jetting (Multi/PolyJet), stereolithography (SLA) and Selective Laser Sintering (SLS) which offer comparative resolutions in the range of 0.02mm and create smoother finishes [4939,6050]. FDM prints are also limited by shell artifacts whereby sudden transitions in attenuation at the rim of the printed parts limits the realism of homogenous tissue backgrounds. Furthermore, an infill percentage below 40% results in visible and unrealistic print patterns on CT [22].

Material Jetting uses an inkjet head to successively eject droplets of photopolymers which are selectively cured using ultraviolet light to build a 3D construct. SLA selectively cures a vat of photocurable resin [8], while SLS employs a laser to selectively fuse regions of a powder bed [5949]. Finer spatial resolutions may explain why studies utilised these methods predominantly for printing small nodules [3626,4535,4636] and underlay the challenges Hatamikia et al. [3323] faced in replicating accurate geometries of smaller lung nodules when employing FDM printing methods. Nonetheless, studies that utilised material jetting and SLS suffered from longer printing times, expensive resources, and laborious modelling steps due to requiring support materials with subsequent removal [3525-3727]. The limited selection of photopolymers available additionally constrains the range of radiodensities achievable with these methods [2]. Advantages and disadvantages of a selection of materials investigated in this review is presented in Table 4. .

Formatted: Font color: Auto

Formatted: Font color: Auto

Formatted: Font color: Auto

Formatted: Font color: Auto

Formatted: Font color: Auto

Table 4. Comparison of 3D printing materials presented in this review.

Formatted: Font: Bold

Material (Printing Method)	**Advantages**	**Disadvantages**
PLA (FDM)	Low melting point [59] Simple print process [32] Non-toxic and biocompatible [59] Rigid and strong [60] Wide variety of colours [59] Inexpensive and highly available [59] Suitable for soft tissue and muscle replication as exhibits radiodensities between 32-185 HU at 100% infill [40,42, 45]	Brittle [59] Rough surface finnish [59] Surface texture is unnatural due to laminae or stair-step appearance [43] Low heat resistance – can warp and melt under sun exposure [61] Prone to oozing effect [61] FDM requires removal of support material for overhanging parts [62]
ABS (FDM)	Relatively low attenuations, making it suitable as a surrogate for adipose tissue [40] Tough, and impact resistant, makes for robust molders to encase filler materials [39]	Prone to shrinkage and warping during cooling after the print [40] Requires removal of support material for overhanging parts [62] Toxic [28] Affected by humidity [28]
TPU (FDM and SLS)	Flexible polymer [63] Low radiodensities of around -200HU, suitable for representing subsololid, minimally attenuating lesions [38] Higher resolution enabled with SLS as compared to FDM printing [63]	TPU used with FDM printers is not functionally strong as compared to SLS [63]
Nylon/Polyamide 12 (SLS)	High detail resolution and strength. Suitable for small structures requiring low radiodensities (~-700 to -130HU) [36] Does not require support material due to free powder acting as the support material [36]	Free unsintered poweder may remain trapped in parts of the model [36] High cost printers [36] Prone to thermal distortion [36] Rough and grainy surface finish [36]

Formatted: Font: Bold, Not Italic
Formatted: Font: Bold, Not Italic
Formatted
Formatted
Formatted
Formatted
Formatted
Formatted
Formatted
Formatted
Formatted
Formatted
Formatted
Formatted
Formatted
Formatted: Font: Bold, Not Italic
Formatted
Formatted
Formatted
Formatted
Formatted
Formatted
Formatted: Font: Bold, Not Italic
Formatted
Formatted
Formatted
Formatted
Formatted: Font: Bold, Not Italic
Formatted
Formatted
Formatted
Formatted
Formatted
Formatted

PETG (FDM)	Suitable for cartilage tissue, exhibiting ~170 ± 20 HU [40] Simple to print, flexible and strong [60] Glossy and smooth surface finish [60] Negligible warping [60] Water resistant [60]	Easily scratched and absorbs moisture [59] Can produce thin hairs on surface due to stringing (oozing material) [60]
Vero PureWhite (PolyJet)	Rigid radiopaque photopolymer[64] Fine resolution and accuracy [64] Durable [64] Suitable for moulds encapsulating materials [35]	Brittle [64]
Fillaments doped with high density additives - StoneFill PLA, PLA with iron, granite-PLA, ABS with added Bismuth (FDM), Bone meal powder amalgamate (casting)	Higher aromic numbers and densities enabled to better replicate radiodensities of cortical bone, which is not achievable with base polymer materials [10]. StoneFil PLA – density of 1.54 g/cm³ [10]	Long-term damage of the extrusion nozzle due to abrasion from high density additives [8]. bone meal amalgamate casting requires more than 24hrs to cure, introduces air bubble artifacts and necessitates a sealed compartment to prevent leaking into neighbouring areas. These considerations are relevant to casting in general [35]
VisiJet EX200 (Multi-Jet)	Very tough and durable [65] Transparent – allows visualisation of internal structures [66] High resolution – enables smooth curves or sharp edges [67] Biocompatible [68]	May cause skin irritation [69] Slight odour [69] Requires support material for overhanging structures [64] Expensive ~~P~~printer [37]
Gypsum Powder (Binder Jetting)	Low cost and accessible [70] High Density of 1.57 g/cm³, gives radiodensities between 372-995HU, similar to bone [10,36]	Low strength [70] Porous [70]
PMMA (FDM)	Transparent – allows visualisation of internal structures [71]	Shrinks and warps without a heated printing bed [71]

	Strong and durable [71] Resistance to UV and other weather exposures [71] Density of 1.12g/cm³ [10]. Suitable radiodensity for glandular tissue at ~95HU [35]	Harmful gasses emitted during printing – requires good ventillation [71]
Silicone of the FlexFoam-IT series (casting) [72]	Expandable and durable, suitable densities for representing skin and lung parenchyma according to expansion factor [39] Silicone of the FlexFoam-IT series has short curing time of less than 2 hrs [34]. Silicone Dragon Skin has a long shelf-life and fast curing time (<16 hrs) [36]	Pot life of only 1 minute after opening [39] Requires a silicone releasing agent in order to remove the mold [39] Requires a completely sealed mold in order to avoid leaking into neighbouring areas [35]

Formatted: Font color: Auto
Formatted: Font: Not Italic, Font color: Auto
Formatted: Font color: Auto
Formatted: Font: Not Italic, Font color: Auto
Formatted: Font color: Auto
Formatted: Font: Not Italic, Font color: Auto
Formatted: Font color: Auto
Formatted: Font: Not Italic, Font color: Auto
Formatted: Font color: Auto
Formatted: Font: Not Italic, Font color: Auto
Formatted: Font: Not Italic
Formatted: Font: Not Italic, Font color: Auto
Formatted: Font: Not Italic, Font color: Auto
Formatted: Font color: Auto
Formatted: Font: Not Italic, Font color: Auto
Formatted: Font: Not Italic
Formatted: Font color: Auto
Formatted: Font: Not Italic, Font color: Auto
Formatted: Font color: Auto
Formatted: Font: Not Italic, Font color: Auto
Formatted: Font color: Auto
Formatted: Font: Not Italic, Font color: Auto
Formatted: Left
Formatted: Font color: Auto
Formatted: Font: Not Italic, Font color: Auto
Formatted: Font color: Auto
Formatted: Font: Not Italic, Font color: Auto
Formatted: Font color: Auto
Formatted: Font: Not Italic, Font color: Auto

4.3 3D printing thoracic organs

Current literature has mostly investigated the creation of discrete thoracic organs with limited consideration of comprehensive chest phantoms. For example, Abdullah at al., [3020] printed a single heart, Morup et al. [1811] developed 3D printed coronary arteries, Hong et al. [3929] produced an aorta and Aldosari et al. [3121] created pulmonary arteries. Likewise, Hatamikia et al. [3424,3525] solely investigated the bony thorax, without inclusion of other thoracic structures. Additionally, skin, subcutaneous fat and muscle structures tend to not be delineated into their sub-structures, and rather printed as a single soft-tissue structure with homogenous radiodensity [3626,3727,4030,4131].

Hong et al. [3929] produced the most comprehensive model of all studies, incorporating 7 thoracic structures: skin, fat, muscle, bone, heart, lung, and parenchymal lesions. Despite achieving radiation equivalence, the radiation attenuating properties of the heart was not evaluated, and the phantom merely represented an axial slice rather than comprising the entire torso. Cavaliere et al. [3222] produced a comprehensive thoracic model built with a single material (PLA), however, the phantom did not achieve radiation or geometrical equivalence. Tissue attenuations are impacted by surrounding tissues and structures due to beam hardening, thus limiting the application and generalisability of these single organ studies and phantoms with unrealistic tissue backgrounds [5242]. This warrants further studies investigating comprehensive, holistic, and more realistic thoracic models.

Thoracic phantoms described in the literature predominantly consist of lung replicas, created using a variety of materials, including PLA (infill rates of 10%, 30%, 46% and 100%), ABS (50%), TPU (50%), Nylon, low-density paper, and foamed silicone gels [3222,3626,3828-4232,4434]. Lung phantoms mostly achieved radiation equivalence within the norms of pulmonary parenchyma, which ranges between -700 to -900HU [7351]. However, most of the models did not include blood vessels and struggled to match the low radiodensity of aerated lung tissue (<-1000HU [3222,7351]), achieving an average radiodensity of -610HU (-417 to -933HU). Underlying this challenge is the requirement for 3D constructs to have a printing scaffold and to maintain structural integrity, which limits the reduction of infill rates and presence of large air gaps [3222]. Furthermore, minimum attenuations are ascribed by the intrinsic properties of the base material as revealed by Wang et al.'s [4636] paper-based lung model which was unable to replicate aerated lung densities. PLA with 10% infill produced the closest approximation to aerated lung tissue (-933HU) [3222].

Similarly, studies faced challenges in replicating the higher attenuations of bone (>1000HU [5848]), as the raw materials used typically fall within the soft tissue density range [3222,3828,5145]. PLA doped with 50% iron achieved the highest attenuations, closest to dense cortical bone [4131]. The high atomic number and electron density of iron make it an ideal additive for increasing the attenuation of PLA composite materials, primarily due to the enhanced occurrence of the photoelectric effect [5242,5545]. Stone filledd filaments as well as radiopaque substances were additionally employed, however, achieved relatively lower attenuations, likely due to lower densities and mal absorption of contrast [3429,5145]. Similarly, Ceh et al. -[7452] used a Bismuth doped ABS filament in their 3D printed nasocranial phantom, achieving radiodensity between 1000-3000HU. Thus, incorporation of filaments with mixed metallic and high-density additives shows promise for improving replication of bone-like attenuations in thoracic phantoms [3222,5545]. However, over time, dense metal particles can abrade the printer nozzle, leading to imperfections in the 3D object with different attenuations and geometries [5545].

Studies that printed lung lesions included between 1-12 nodules, created using pearl-powder solution, PLA, Silicone foam, Nylon, Acrylonitrile Styrene Acrylate (ASA), Acrylonitrile Butadiene Styrene (ABS) and Polyethylene terephthalate glycol (PETG) of varying infill percentages [3222,3323,3626,3828,3929,4535,4636,4838]. These studies achieved radiodensitiesradiodensities between -909 to 227HU, representing sub-solid and solid

Formatted: Font color: Auto

Formatted: Font color: Auto

Formatted: Font color: Auto

Formatted: Font color: Auto

Formatted: Font color: Auto

nodules, employing printing methods including SLA, FDM, Binder Jetting and SLS. The selection of SLA, SLS, and binder jetting over FDM in some studies likely aimed to achieve finer details due to their higher printing resolution, despite the associated higher costs of these techniques [3626,4535].

Printed lung nodules in phantoms served multiple purposes, including feasibility assessment for creating tissue equivalent radiodensities [3828,3929], validation of imaging algorithms [283], quality analysis of X-ray images [3626] and to compare the detection sensitivity of paediatric lung nodules using different image reconstruction methods [4535]. However, no study utilised these phantoms for optimising low dose protocols for lung cancer screening, such as modifying kVp and mAs acquisition parameters, revealing a potential avenue for further research. Furthermore, this review underscores that the use of 3D-printed thoracic phantoms for optimizing low-dose protocols has predominantly been explored in the cardiovascular field [180, 2818, 2919], indicating a need to expand such investigations into the realm of pulmonary imaging and screening protocols.

Another limitation of these 3D printed chest phantoms is their inability to simulate physiological conditions such as dynamic cardiovascular systems with haemodynamic flow, heartbeat, and lung movements during breathing. This has implications for image quality for example by creating movement artifacts and distributing dose differently in moving tissues [7553]. Although challenging, addressing these tasks in future studies is worthwhile. Advancements in 3D and 4D bioprinting, which aim to replicate the structural and functional heterogeneity of tissue constructs using seeded stem cells or biomimetic multi-materials, is a possible avenue for achieving this feat [76]. ~~Advancements in 3D and 4D bioprinting which aims to replicate the structural and functional heterogeneity of tissue constructs using seeded stem cells, is a possible avenue for achieving this feat.~~

5. Conclusion

In conclusion, this review highlights the rapid advancements of 3D-printed, patient-specific thoracic phantoms in radiology and medical imaging within the past six years. A versatile array of discreteet thoracic organs has been printed, primarily via the affordable means of fused deposition modelling. While efforts have been made to fabricate comprehensive chest phantoms, there remains a notable gap in the representation of essential thoracic structures. While many studies have focused on demonstrating the feasibility of 3D printing for anthropomorphic and tissue-equivalent thoracic phantoms, further investigations are warranted to explore their broader applications in radiology and medical imaging. The prevalence of cardiovascular phantoms for optimizing low-dose protocols emphasises the need for expanding research into pulmonary applications. Specifically, the development and utilization of comprehensive, three-dimensional printed patient-specific models for optimizing low-dose lung cancer screening protocols represents an important area that requires more attention and investigation. Therefore, we recommend developing a 3D printed chest model to optimise CT protocols for lung cancer screening.

Author Contributions: Conceptualization, J.S. and Z.S.; methodology, J.S.; formal analysis, J.S.; data curation, J.S.; writing—original draft preparation, J.S.; writing—review and editing, Z.S. and J.S.; visualization, J.S, and Z.S.; supervision, Z.S. All authors have read and agreed to the published version of the manuscript.

Funding: This research received no external funding.

Institutional Review Board Statement: Not applicable.

Informed Consent Statement: Not applicable.

Data Availability Statement: Not applicable.

Formatted: Font color: Auto

Conflicts of Interest: The authors declare no conflicts of interest. 583

References

1. Sun, Z.; Wong, Y.H.; Yeong, C.H. Patient-specific 3D-printed low-cost models in medical education and clinical practice. *Micromachines.* **2023**, *14*, 464. doi:10.3390/mi14020464.
2. Farooqi, K.M. Rapid prototyping technologies In *Rapid Prototyping in Cardiac Disease;* Borrello, J., Backeris, P.,Eds.; Springer International Publishing. AG Switzerland, 2017; pp. 41-49.
3. Rossi, T.; Williams, A.; Sun, Z. Three-Dimensional Printed Liver Models for Surgical Planning and Intraoperative Guidance of Liver Cancer Resection: A Systematic Review. *Appl. Sci.* **2023**, *13*, 10757, doi:10.3390/app131910757.
4. Ghantous, Y.; Nashef, A.; Mohanna, A.; Abu-El-naaj, I. Three-dimensional technology applications in maxillofacial reconstructive surgery: Current surgical implications. *Nanomaterials.* **2020**, *10*, 2523, doi:10.3390/nano10122523.
5. Haleem, A.; Javaid, M.; Suman, R.; Singh, R.P. 3D printing applications for radiology: an overview. *Indian J. Radiol. Imaging.* **2021**, *31*, 010-017, doi:10.1055/s-0041-1729129.
6. Filippou, V.; Tsoumpas, C. Recent advances on the development of phantoms using 3D printing for imaging with CT, MRI, PET, SPECT, and ultrasound. *J. Med. Phys.* **2018**, *45*, e740-e760, doi:10.1002/mp.13058.
7. Scalzetti, E.M.; Huda, W.; Bhatt, S.; Ogden, K.M. A method to obtain mean organ doses in a Rando phantom. *Health. Phys.* **2008**, *95*, 241-244, doi:10.1097/01.HP.0000310997.09116.e3.
8. Okkalidis, N. 3D printing methods for radiological anthropomorphic phantoms. *Phys. Med. Biol.* **2022**, *67*, 15TR04, doi:10.1088/1361-6560/ac80e7.

~~8.~~9. Ma, X.; Figl, M.; Unger, E.; Buschmann, M.; Homolka, P. X-ray attenuation of bone, soft and adipose tissue in CT from 70 to 140 kV and comparison with 3D printable additive manufacturing materials. *Sci. Rep.* **2022**, *12*, 14580, doi:10.1038/s41598-022-18741-4.

~~9.~~10. Kunert, P.; Trinkl, S.; Giussani, A.; Reichert, D.; Brix, G. Tissue equivalence of 3D printing materials with respect to attenuation and absorption of X-rays used for diagnostic and interventional imaging. *J. Med. Phys.* **2022**, *49*, 7766-7778, doi:10.1002/mp.15987.

11. Tino, R.; Yeo, A.; Leary, M.; Brandt, M.; Kron, T. A Systematic Review on 3D-Printed Imaging and Dosimetry Phantoms in Radiation Therapy. *Technol. Cancer. Res. Treat.* **2019**, *18*, 1533033819870208, doi:10.1177/1533033819870208.
12. Germann, M.; Shim, S.; Angst, F.; Saltybaeva, N.; Boss, A. Spiral breast computed tomography (CT): signal-to-noise and dose optimization using 3D-printed phantoms. *Eur. J. Radiol.* **2021**, 31, 3693-3702, doi:10.1007/s00330-020-07549-3.
13. Jahnke, P.; Schwarz, S.; Ziegert, M.; Schwarz, F.B.; Hamm, B.; Scheel, M. Paper-based 3D printing of anthropomorphic CT phantoms: Feasibility of two construction techniques. *Eur. J. Radiol.* **2019**, 29, 1384-1390, doi:10.1007/s00330-018-5654-1.
14. Irnstorfer, N.; Unger, E.; Hojreh, A.; Homolka, P. An anthropomorphic phantom representing a prematurely born neonate for digital x-ray imaging using 3D printing: Proof of concept and comparison of image quality from different systems. *Sci. Rep.* **2019**, *9*, 14357, doi:10.1038/s41598-019-50925-3.
15. Homolka, P.; Figl, M.; Wartak, A.; Glanzer, M.; Dünkelmeyer, M.; Hojreh, A.; Hummel, J. Design of a head phantom produced on a 3D rapid prototyping printer and comparison with a RANDO and 3M lucite head phantom in eye dosimetry applications. *Phys. Med. Biol.* **2017**, 62, 3158-3174, doi:10.1088/1361-6560/aa602
16. Rossman, A.H.; Catenacci, M.; Zhao, C.; Sikaria, D.; Knudsen, J.E.; Dawes, D.; Gehm, M.E.; Samei, E.; Wiley, B.J.; Lo, J.Y. Three-dimensionally-printed anthropomorphic physical phantom for mammography and digital breast tomosynthesis with custom materials, lesions, and uniform quality control region. *J. Med. Imaging.* **2019**, 6, 021604-021604, doi:10.1117/1.JMI.6.2.021604.

~~10.~~17. Tong, H.; Pegues, H.; Samei, E.; Lo, J.Y.; Wiley, B.J. Controlling the attenuation of 3D-printed physical phantoms for computed tomography with a single material. *Med.Phys.* **2022**, 49, 2582-2589, doi:10.1002/mp.15494.

~~11.~~18. Mørup, S.D.; Stowe, J.; Precht, H.; Gervig, M.H.; Foley, S. Design of a 3D printed coronary artery model for CT optimization. *Radiography.* **2022**, *28*, 426-432, doi:10.1016/j.radi.2021.09.001.

~~12.~~19. Sindi, R.; Wong, Y.H.; Yeong, C.H.; Sun, Z. Development of patient-specific 3D-printed breast phantom using silicone and peanut oils for magnetic resonance imaging. *Quant. Imaging. Med. Surg.* **2020**, *10*, 1237-1248, doi:10.21037/qims-20-251.

20. Kang, S.-H.; Park, M.; Yoon, M.S.; Lee, Y. Quantitative evaluation of total variation noise reduction algorithm in CT images using 3D-printed customized phantom for femur diagnosis. *J. Korean. Phys. Soc.* **2022**, *81*, 450-459, doi:10.1007/s40042-022-00515-w.

~~13.~~21. Li, X.; Wu, B.; Zou, Y.; Zhang, G.; Liu, S.; Zhao, L.; Zhang, Z.; Wu, W.; Liu, C.; Ai, S. Development of a 3D-printed pelvic CT phantom combined with fresh pathological tissues of bone tumor. *Quant. Imaging. Med. Surg.* **2022**, 12, 4647-4657, doi:10.21037/qims-22-147.

~~14.~~22. Leitão, C.A.; Salvador, G.L.d.O.; Tazoniero, P.; Warszawiak, D.; Saievicz, C.; Jakubiak, R.R.; Escuissato, D.L. Dosimetry and comparison between different CT protocols (low dose, ultralow dose, and conventional CT) for lung nodules' detection in a phantom. *Radiol. Res. Pract.* **2021**, *2021*, doi:10.1155/2021/6667779.

Formatted: Font: Italic
Formatted: Font: Bold
Formatted: Font: Bold
Formatted: English (United States)
Formatted: Font: Italic
Formatted: Font: Bold
Formatted: Font: Italic
Formatted: Font: Bold
Formatted: Font: Italic
Formatted: Font: Bold
Formatted: Left
Formatted: Font: Bold

15.23. Huber, A.; Landau, J.; Ebner, L.; Bütikofer, Y.; Leidolt, L.; Brela, B.; May, M.; Heverhagen, J.; Christe, A. Performance of ultralow-dose CT with iterative reconstruction in lung cancer screening: limiting radiation exposure to the equivalent of conventional chest X-ray imaging. *Eur. Radiol.* **2016**, *26*, 3643-3652, doi:10.1007/s00330-015-4192-3.

24. Mascalchi, M.; Picozzi, G.; Puliti, D.; Diciotti, S.; Deliperi, A.; Romei, C.; Falaschi, F.; Pistelli, F.; Grazzini, M.; Vannucchi, L.; et al. Lung Cancer Screening with Low-Dose CT: What We Have Learned in Two Decades of ITALUNG and What Is Yet to Be Addressed. *Diagnostics.* **2023**, *13*, doi:10.3390/diagnostics13132197.

25. McCollough, C.H.; Leng, S. Use of artificial intelligence in computed tomography dose optimisation. *Annals of the ICRP.* **2020**, 49, 113-125, doi:10.1177/0146645320940827.

16.26. Hsieh, J.; Flohr, T. Computed tomography recent history and future perspectives. *J Med Imaging.* **2021**, *8*, 052109, doi:10.1117/1.Jmi.8.5.052109.

17.27. Liberati, A.; Altman, D.G.; Tetzlaff, J.; Mulrow, C.; Gotzsche, P.C.; Ioannidis, J.P.A.; Clarke, M.; Devereaux, P.J.; Kleijnen, J.; Moher, D. The PRISMA statement for reporting systematic reviews and meta-analyses of studies that evaluate healthcare interventions: explanation and elaboration. *BMJ (Online).* **2009**, *339*, doi:10.1136/bmj.b2700.

18.28. Cano-Vicent, A.; Tambuwala, M.M.; Hassan, S.S.; Barh, D.; Aljabali, A.A.A.; Birkett, M.; Arjunan, A.; Serrano-Aroca, Á. Fused deposition modelling: Current status, methodology, applications and future prospects. *Addit. Manuf.* **2021**, *47*, 102378, doi:10.1016/j.addma.2021.102378.

19.29. Crowe, M.; Sheppard, L.; Campbell, A. Reliability analysis for a proposed critical appraisal tool demonstrated value for diverse research designs. *J. Clin. Epidemiol.* **2012**, *65*, 375-383, doi:10.1016/j.jclinepi.2011.08.006.

20.30. Abdullah, K.A.; McEntee, M.F.; Reed, W.; Kench, P.L. Development of an organ-specific insert phantom generated using a 3D printer for investigations of cardiac computed tomography protocols. *J. Med. Radiat. Sci.* **2018**, *65*, 175-183, doi:10.1002/jmrs.279.

21.31. Aldosari, S.; Jansen, S.; Sun, Z. Patient-specific 3D printed pulmonary artery model with simulation of peripheral pulmonary embolism for developing optimal computed tomography pulmonary angiography protocols. *Quant. Imaging. Med. Surg.* **2019**, *9*, 75-85, doi:10.21037/qims.2018.10.13.

22.32. Cavaliere, C.; Baldi, D.; Brancato, V.; Aiello, M.; Salvatore, M. A customized anthropomorphic 3D-printed phantom to reproducibility assessment in computed tomography: an oncological case study. *Front. Oncol.* **2023**, *13*, 1123796, doi:10.3389/fonc.2023.1123796.

23.33. Hatamikia, S.; Gulyas, I.; Birkfellner, W.; Kronreif, G.; Unger, A.; Oberoi, G.; Lorenz, A.; Unger, E.; Kettenbach, J.; Figl, M.; et al. Realistic 3D printed CT imaging tumor phantoms for validation of image processing algorithms. *Phys. Med.* **2023**, *105*, doi:10.1016/j.ejmp.2022.102512.

24.34. Hatamikia, S.; Kronreif, G.; Unger, A.; Oberoi, G.; Jaksa, L.; Unger, E.; Koschitz, S.; Gulyas, I.; Irnstorfer, N.; Buschmann, M.; et al. 3D printed patient-specific thorax phantom with realistic heterogenous bone radiopacity using filament printer technology. *J. Med. Phys.* **2022**, *32*, 438-452, doi:10.1016/j.zemedi.2022.02.001.

25.35. Hatamikia, S.; Oberoi, G.; Unger, E.; Kronreif, G.; Kettenbach, J.; Buschmann, M.; Figl, M.; Knäusl, B.; Moscato, F.; Birkfellner, W. Additively Manufactured Patient-Specific Anthropomorphic Thorax Phantom With Realistic Radiation Attenuation Properties. *Front. Bioeng. Biotechnol.* **2020**, *8*, 385, doi:10.3389/fbioe.2020.00385.

26.36. Hazelaar, C.; Eijnatten, M.; Dahele, M.; Wolff, J.; Forouzanfar, T.; Slotman, B.; Verbakel, W.F.A.R. Using 3D printing techniques to create an anthropomorphic thorax phantom for medical imaging purposes. *J. Med. Phys.* **2018**, *45*, 92-100, doi:10.1002/mp.12644.

27.37. Hernandez-Giron, I.; den Harder, J.M.; Streekstra, G.J.; Geleijns, J.; Veldkamp, W.J.H. Development of a 3D printed anthropomorphic lung phantom for image quality assessment in CT. *Phys. Med.* **2019**, *57*, 47-57, doi:10.1016/j.ejmp.2018.11.015.

28.38. Hong, D.; Lee, S.; Kim, G.B.; Lee, S.M.; Kim, N.; Seo, J.B. Development of a CT imaging phantom of anthromorphic lung using fused deposition modeling 3D printing. *Medicine (Baltimore).* **2020**, *99*, e18617, doi:10.1097/md.0000000000018617.

29.39. Hong, D.; Moon, S.; Seo, J.B.; Kim, N. Development of a patient-specific chest computed tomography imaging phantom with realistic lung lesions using silicone casting and three-dimensional printing. *Sci. Rep.* **2023**, *13*, 3941, doi:10.1038/s41598-023-31142-5.

30.40. Kunert, P.; Schlattl, H.; Trinkl, S.; Giussani, A.; Klein, L.; Janich, M.; Reichert, D.; Brix, G. Reproduction of a conventional anthropomorphic female chest phantom by 3D-printing: Comparison of image contrasts and absorbed doses in CT. *J. Med. Phys.* **2023**, *50*, 4734-4743, doi:10.1002/mp.16587.

31.41. Mille, M.M.; Griffin, K.T.; Maass-Moreno, R.; Lee, C. Fabrication of a pediatric torso phantom with multiple tissues represented using a dual nozzle thermoplastic 3D printer. *J. Appl. Clin. Med. Phys.* **2020**, *21*, 226-236, doi:10.1002/acm2.13064.

32.42. Okkalidis, N. A novel 3D printing method for accurate anatomy replication in patient-specific phantoms. *J. Med. Phys.* **2018**, *45*, 4600-4606, doi:10.1002/mp.13154.

33.43. Shapira, N.; Donovan, K.; Mei, K.; Geagan, M.; Roshkovan, L.; Gang, G.J.; Abed, M.; Linna, N.B.; Cranston, C.P.; O'Leary, C.N.; et al. Three-dimensional printing of patient-specific computed tomography lung phantoms: a reader study. *PNAS. Nexus.* **2023**, *2*, pgad026, doi:10.1093/pnasnexus/pgad026.

Formatted: Font: Italic

Formatted: Font: Bold

~~34.~~44. Shapira, N.; Donovan, K.; Mei, K.; Geagan, M.; Roshkovan, L.; Litt, H.I.; Gang, G.J.; Stayman, J.W.; Shinohara, R.T.; Noël, P.B. PixelPrint: Three-dimensional printing of realistic patient-specific lung phantoms for CT imaging. *Proc. SPIE. Int. Soc. Opt. Eng.* **2022**, *12031*, doi:10.1117/12.2611805.

~~35.~~45. Shim, J.; Yoon, M.; Lee, Y. Comparison of filtered back projection with fast non-local means denoising approach and iterative reconstruction in pediatric chest CT image using 3D printed lung nodules. *J. Korean Phys. Soc.* **2023**, *82*, 1114-1123, doi:10.1007/s40042-023-00757-2.

~~36.~~46. Wang, J.; Falkson, S.R.; Guo, H.H. Radiopaque Recreations of Lung Pathologies from Clinical Computed Tomography Images Using Potassium Iodide Inkjet 3-dimensional Printing: Proof of Concept. *J. Thorac. Imaging.* **2022**, *37*, 146-153, doi:10.1097/RTI.0000000000000607.

~~37.~~47. Wu, C.A.; Squelch, A.; Jansen, S.; Sun, Z. Optimization of computed tomography angiography protocols for follow-up type b aortic dissection patients by using 3d printed model. *Appl. Sci.* **2021**, *11*, doi:10.3390/app11156844.

~~38.~~48. Zhang, F.; Zhang, H.; Zhao, H.; He, Z.; Shi, L.; He, Y.; Ju, N.; Rong, Y.; Qiu, J. Design and fabrication of a personalized anthropomorphic phantom using 3D printing and tissue equivalent materials. *Quant. Imaging. Med. Surg.* **2019**, *9*, 94-100, doi:10.21037/qims.2018.08.01.

~~39.~~49. George, E.; Liacouras, P.; Rybicki, F.J.; Mitsouras, D. Measuring and Establishing the Accuracy and Reproducibility of 3D Printed Medical Models. *Radiographics.* **2017**, *37*, 1424-1450, doi:10.1148/rg.2017160165.

~~40.~~50. Wu, C.-A.; Squelch, A.; Sun, Z. Investigation of three-dimensional printing materials for printing aorta model replicating type B aortic dissection. *Curr. Med. Imaging. Rev.* **2021**, *17*, 843-849, doi:10.2174/1573405617666210218102046.

~~41.~~51. Sorooshfard, E.; Tahmasbi, M.; Chegeni, N.; Birgani, M.J.T. Evaluating the effects of variation in CT scanning parameters on the image quality and Hounsfield units for optimization of dose in radiotherapy treatment planning: A semi-anthropomorphic thorax phantom study. *JCRT.* **2023**, *19*, doi:10.4103/jcrt.jcrt_260_21.

52. Dowsett, D.; Kenny, P.; Johnston, E. Interactions of X- and gamma radiation with matter. In *The Physics of Diagnostic Imaging*, 2nd ed.; Dowsett, D., Kenny, P., Johnston, E., Eds.; CRC Press: London, 2012; pp. 113-141.

~~42.~~

~~43.~~53. Koyotokagaku. Product Data: Multipurpose Chest Phantom N1 "LUNGMAN". Available online: https://www.kyoto-kagaku.com/en/products_data/ph-1_01/ (accessed on 25 April 2024).

~~44.~~54. Ma, X.; Buschmann, M.; Unger, E.; Homolka, P. Classification of X-ray attenuation properties of additive manufacturing and 3D printing materials using computed tomography from 70 to 140 kVp. *Front. bioeng. biotechnol.* **2021**, *9*, 763960, doi:10.3389/fbioe.2021.763960.

~~45.~~55. Madison, K.; Weygand, J.; Andreozzi, J.M.; Hunt, D.; Perez, B.A.; Graham, J.A.; Gage, R. Methodology for computed tomography characterization of commercially available 3D printing materials for use in radiology/radiation oncology. *J. Appl. Clin. Med. Phys.* **2023**, *24*, doi:10.1002/acm2.13999.

~~46.~~56. Savi, M.; Andrade, M.A.B.; Potiens, M.P.A. Commercial filament testing for use in 3D printed phantoms. *Radiat. Phys. Chem. Oxf. Engl. 1993* **2020**, *174*, 108906, doi:10.1016/j.radphyschem.2020.108906.

57. van Eijnatten, M.; Koivisto, J.; Karhu, K.; Forouzanfar, T.; Wolff, J. The impact of manual threshold selection in medical additive manufacturing. *Int. J. Comput. Assist. Radiol. Surg.* **2017**, *12*, 607-615, doi:10.1007/s11548-016-1490-4.

58. Mei, K.; Geagan, M.; Roshkovan, L.; Litt, H.I.; Gang, G.J.; Shapira, N.; Stayman, J.W.; Noël, P.B. Three-dimensional printing of patient-specific lung phantoms for CT imaging: emulating lung tissue with accurate attenuation profiles and textures. *J. Med. Phys.* **2022**, *49*, 825-835, doi:10.1002/mp.15407.

~~47.~~59. Ligon, S.C.; Liska, R.; Stampfl, J.; Gurr, M.; Mülhaupt, R. Polymers for 3D Printing and Customized Additive Manufacturing. *Chem. Rev.* **2017**, *117*, 10212-10290, doi:10.1021/acs.chemrev.7b00074.

60. Gharleghi, R.; Dessalles, C.A.; Lal, R.; McCraith, S.; Sarathy, K.; Jepson, N.; Otton, J.; Barakat, A.I.; Beier, S. 3D Printing for Cardiovascular Applications: From End-to-End Processes to Emerging Developments. *Ann. Biomed. Eng.* **2021**, *49*, 1598-1618, doi:10.1007/s10439-021-027841

61. Iftekar, S.F.; Aabid, A.; Amir, A.; Baig, M. Advancements and Limitations in 3D Printing Materials and Technologies: A Critical Review. *Polymers.* **2023**, 15, 2519. doi: 10.3390/polym15112519

62. Formlabs. Guide to 3D Printing Materials: Types, Applications, and Properties. Available online: https://formlabs.com/asia/blog/3d-printing-materials/ (accessed on 16 June 2024).

63. Simplify3D. Filament Properties Table. Available online: https://www.simplify3d.com/resources/materials-guide/properties-table/ (accessed on 16 June 2024).

64. Barile, G.; Leoni, A.; Muttillo, M.; Paolucci, R.; Fazzini, G.; Pantoli, L. Fused-Deposition-Material 3D-Printing Procedure and Algorithm Avoiding Use of Any Supports. *Sensors.* **2020**, *20*, doi:10.3390/s20020470.

65. Formlabs. Flexible 3D Printing Guide: Compare Processes, Materials, and Applications. Available online: https://formlabs.com/blog/flexible-3d-printing-materials-and-processes/ VisiJet® EX200 Plastic Material for 3-D Modeling (accessed on 16 June 2024).

Formatted: Font: Italic

Formatted: Font: Bold

Formatted: Default Paragraph Font

Formatted: Font: Bold, English (Australia)

Formatted: Default Paragraph Font

Formatted: English (United States)

Formatted: English (United States)

Formatted: Default Paragraph Font

Formatted: English (United States)

66. Majca-Nowak, N.; Pyrzanowski, P. The Analysis of Mechanical Properties and Geometric Accuracy in Specimens Printed in Material Jetting Technology. *J. Mater.* **2023**, *16*, doi:10.3390/ma16083014.
67. 3D Systems. VisiJet® EX200 Plastic Material for 3-D Modeling. Available online: https://www.pdmodels.co.uk/datasheets/Visijet_EX200_Info_0509.pdf (accessed on 17 June 2024).
68. 3D Systems. USP Class VI and ISO 10993-1 Information. Available online: https://support.3dsystems.com/s/article/materials-usp-class-vi-and-iso-10993-1-information?language=en_US (accessed on 17 June 2024).
69. 3D Systems. Safety Data Sheet. Available online: https://printer-docs-public.s3.amazonaws.com/sites/default/files/sds-files/professional/VisiJet_EX200/SDS_24184_MTR_UGHS_EN_04-17-2024-VisiJet%20EX%20200%2C%20Visi-Jet%20M3%20Crystal.pdf (accessed on 17 June 2024).
70. Huang, J.; Duan, B.; Cai, P.; Manuka, M.; Hu, H.; Hong, Z.; Cao, R.; Jian, S.; Ma, B. On-demand setting of extrusion-based 3D printing gypsum using a heat-induced accelerator. *Constr. Build. Mater.* **2021**, *304*, 124624, doi: 10.1016/j.conbuildmat.2021.124624.
71. Form Futura 3D Printing Materials. PMMA Filament. Available online: https://formfutura.com/c/filaments/pmma/ (accessed on 17 June 2024).
~~48.~~72. Smooth-On. FlexFoam-iT!™ X. Available online: https://www.smooth-on.com/products/flexfoam-it-x/(accessed on 18 June 2024).
~~49.~~1. ~~Mei, K.; Geagan, M.; Roshkovan, L.; Litt, H.I.; Gang, G.J.; Shapira, N.; Stayman, J.W.; Noël, P.B. Three-dimensional printing of patient-specific lung phantoms for CT imaging: emulating lung tissue with accurate attenuation profiles and textures. *J. Med. Phys.* **2022**, *49*, 825-835, doi:10.1002/mp.15407.~~
~~50.~~1. ~~Ligon, S.C.; Liska, R.; Stampfl, J.; Gurr, M.; Mülhaupt, R. Polymers for 3D Printing and Customized Additive Manufacturing. *Chem. Rev.* **2017**, *117*, 10212-10290, doi:10.1021/acs.chemrev.7b00074.~~
~~51.~~1. ~~Gharleghi, R.; Dessalles, C.A.; Lal, R.; McCraith, S.; Sarathy, K.; Jepson, N.; Otton, J.; Barakat, A.I.; Beier, S. 3D Printing for Cardiovascular Applications: From End-to-End Processes to Emerging Developments. *Ann. Biomed. Eng.* **2021**, *49*, 1598-1618, doi:10.1007/s10439-021-02784-1.~~
~~52.~~73. Seeram, E. *Computed Tomography: Physical Principles, Clinical Applications, and Quality Control*, 3rd ed.; Elsevier: Philadelphia, United States, 2008; pp. 84-102
~~53.~~74. Ceh, J.; Youd, T.; Mastrovich, Z.; Peterson, C.; Khan, S.; Sasser, T.A.; Sander, I.M.; Doney, J.; Turner, C.; Leevy, W.M. Bismuth infusion of ABS enables additive manufacturing of complex radiological phantoms and shielding equipment. *Sensors.* **2017**, *17*, 459, doi:10.3390/s17030459.
75. Gao, L.; Xie, K.; Wu, X.; Lu, Z.; Li, C.; Sun, J.; Lin, T.; Sui, J.; Ni, X. Generating synthetic CT from low-dose cone-beam CT by using generative adversarial networks for adaptive radiotherapy. *J. Radiat. Oncol.* **2021**, *16*, 202, doi:10.1186/s13014-021-01928-w.
~~54.~~76. Chen, A.; Wang, W.; Mao, Z.; He, Y.; Chen, S.; Liu, G.; Su, J.; Feng, P.; Shi, Y.; Yan, C.; et al. Multimaterial 3D and 4D Bioprinting of Heterogenous Constructs for Tissue Engineering. *Adv. Mater.* **2023**, e2307686-e2307686, doi:10.1002/adma.202307686.

Formatted: English (United States)
Formatted: Default Paragraph Font
Formatted: English (United States)
Formatted: Default Paragraph Font
Formatted: Justified
Formatted: Default Paragraph Font
Formatted: English (United States)
Formatted: Font: Italic
Formatted: English (United States)
Formatted: Default Paragraph Font
Formatted: English (United States)
Formatted: Default Paragraph Font, English (United States)
Formatted: Left
Formatted: English (Australia)
Formatted: Font: Bold, English (Australia)